The Thesis Committee for Tianyu Li
Certifies that this is the approved version of the following Thesis:

Modeling of Hydraulic Fracture Propagation and Height Growth in Layered Formations

APPROVED BY
SUPERVISING COMMITTEE:

Jon E. Olson, Supervisor

Mark W. McClure

Modeling of Hydraulic Fracture Propagation and Height Growth in Layered Formations

by

Tianyu Li

Thesis

Presented to the Faculty of the Graduate School of

The University of Texas at Austin

in Partial Fulfillment

of the Requirements

for the Degree of

Master of Science in Engineering

The University of Texas at Austin

December 2018

Dedication

The thesis is dedicated to my daughter Laurel Ruining Chen, who is a naturally born frac'er and a true explorer. I also want to offer thanks to my husband Alfred Chen for all the love and understanding, and my parents, Wenrong and Kaishuang Li, who encouraged me to pursue knowledge from an early age.

Acknowledgements

I would like to thank all the individuals and parties who made the thesis work possible. First and foremost, I want to express my appreciation to my supervisor Dr. Jon Olson. I have been interested in the fracturing topic since my undergraduate years at UT Austin. And after I decided to pursue a higher degree in petroleum engineering, he offered me a really interesting project and accepted me into his research group. While serving a very important role as the department chair, Dr. Olson is always very patient and encouraging in our meetings, and provided me with his ingenious perspectives into the research project. From him, I learned the importance of being optimistic and friendly, and being helpful to students and young professionals. I would also like to thank Dr. Mark McClure for being the second reader of my thesis. Dr. McClure was also my undergraduate research advisor, and he showed me the power of numerical modeling and encouraged me to pursue a master's degree. Special thanks to Dr. Kan Wu, who built the foundational theories of the S3D DDM method, for being supportive and setting an example for our research group.

I want to thank the Fracture Research and Application Consortium (FRAC) for financially supporting this research and providing a platform for academia researchers to communicate ideas with industry leaders. I want to thank all the helpful department staff including but not limited to Dori L. Coy and Amy Stewart for helping me deal with real life questions that cannot be solved by mathematical equation.

I would like to thank my colleagues in the research group for all the inspiring discussions and friendly office atmosphere. Many thanks to Mohsen Babazadeh, Omid

Razavi, Weiwei Wang, Kaimin Yue, Hunjoo Lee, Valerie Gono and Andreas Michael. Last but not least, I want to appreciate the help from all my friends and family.

Abstract

Modeling of Hydraulic Fracture Propagation and Height Growth in Layered Formations

Tianyu Li, M.S.E

The University of Texas at Austin, 2018

Supervisor: Jon E. Olson

Microseismic observations and other field data suggest that hydraulic fractures are often not contained within a single layer. Acoustic log data show rock mechanical properties typically vary significantly between layers, leading to confining stress contrasts across bedding planes. Simulating the propagation of multiple hydraulic fractures in such a multi-layer environment represents a unique challenge when trying to achieve both numerical efficiency and accuracy. Among the concerning factors, fracture height growth and containment is increasingly drawing researchers' attention.

In this master's thesis, an improved simplified 3D (S3D) hydraulic fracture propagation model is developed. The improved model is capable of simulating single and multiple non-planar fracture propagation and height growth in layered reservoir formations with different in-situ stresses, by employing a series of novel methods developed in this study. The S3D displacement discontinuity method (DDM) is extended to model fractures of non-uniform height by applying a new 3D correction factor. A stress correction factor is proposed to calculate the influence of stress contrast between layers on fracture opening.

In the fracture propagation model, fracture width profile along vertical direction in a layered reservoir is calculated by a semi-analytical method introduced in this study. A novel fracture height growth methodology is then developed to predict fracture height in layered formations. The geometric transformation from tip propagation velocity to fracture height growth rate enables the model to avoid common pitfalls of over-predicting the fracture height.

Test cases demonstrate that the improved S3D method can accurately model multiple static fractures with non-uniform fracture height, vertical offset and in-situ stress variation, while maintaining the considerably lower computation time. The proposed improved fracture propagation model is used to simulate the fracture propagation footprint recorded by a fracture experiment. Simulation results from the new fracture propagation model compare favorably with both the experimental data and simulation results from other researchers.

Table of Contents

List of Tables

List of Figures

Chapter 1: Introduction

In this master's thesis, an improved simplified 3D (S3D) hydraulic fracture propagation model is developed. The improved model is capable of simulating single and multiple non-planar fracture propagation and height growth in layered reservoir formations. This chapter provides a general overview of the study, including background and research objective.

1.1 BACKGROUND

The shale revolution in petroleum industry over the last decade is supported by technology developments including hydraulic fracturing and horizontal drilling (Fisher et al., 2004). Hydraulic fracturing is a production stimulation operation to increase reservoir productivity or reduce formation damage effect. Fracturing fluid, primarily water, is injected under high pressure through perforations to create fractures in the rock formation. Successful hydraulic fracturing operations create conductive fractures in low permeability unconventional such as shale. The number of hydraulic fractured horizontal wells has dramatically increased since 2010 and became a majority of U.S. crude oil and natural gas production in late 2014 (Figure 1.1). According to recent studies, hydraulic fracturing accounts for more than half of current U.S. crude oil production (Figure 1.2) and two-thirds of U.S. natural gas production (Figure 1.3).

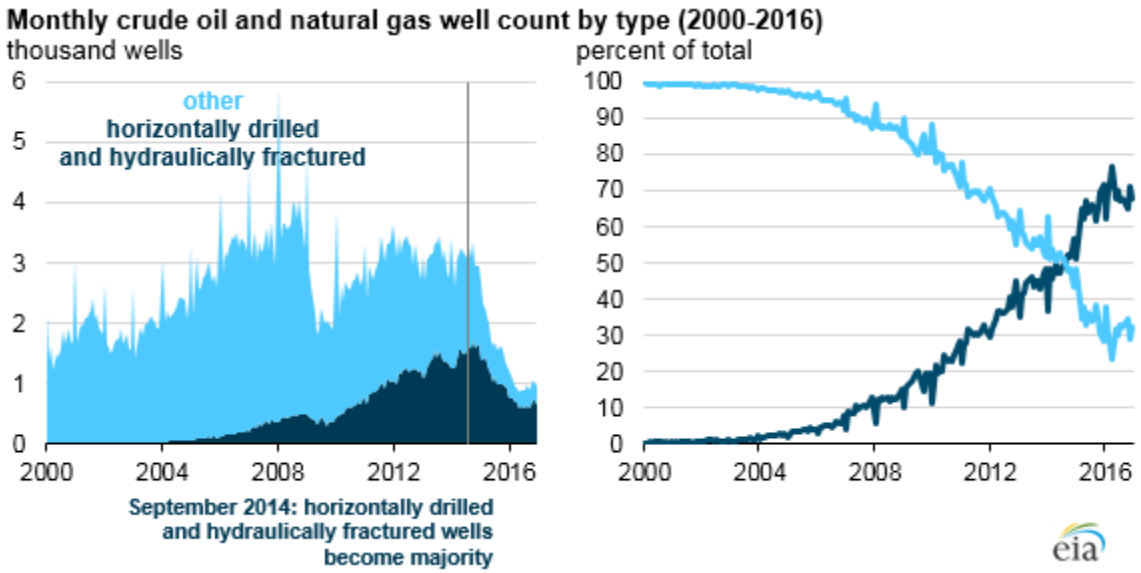

Figure 1.1: U.S. monthly crude oil and natural gas well count by type (U.S. Energy Information Administration, based on DrillingInfo Inc. and IHS Markit, 2018). (https://www.eia.gov/todayinenergy/detail.php?id=34732)

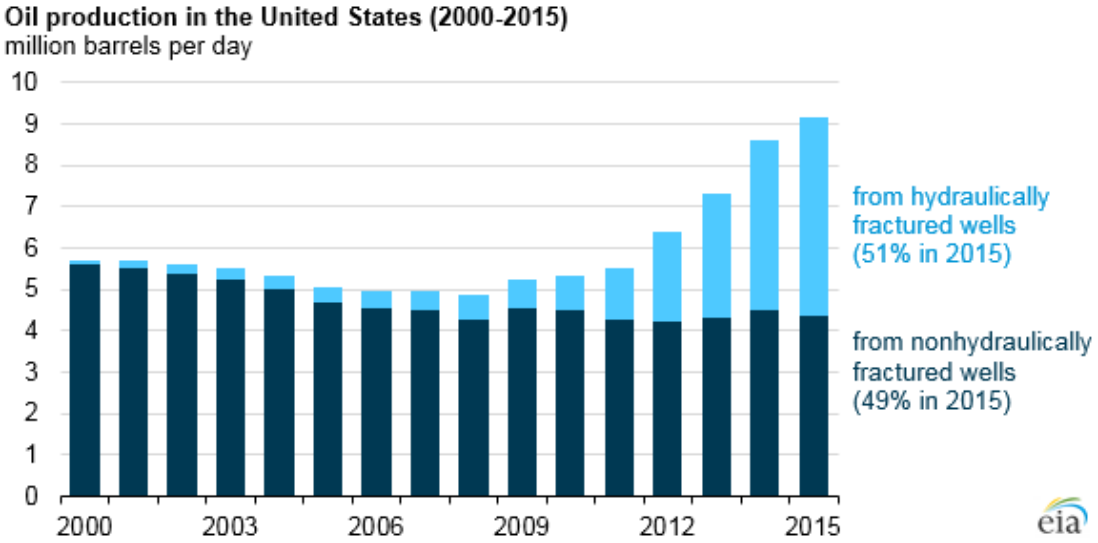

Figure 1.2: U.S. oil production from hydraulically fractured wells and from non-hydraulically fractured wells (2000-2015) (U.S. Energy Information Administration, IHS Global Insight, and DrillingInfo, 2016). (https://www.eia.gov/todayinenergy/detail.php?id=25372)

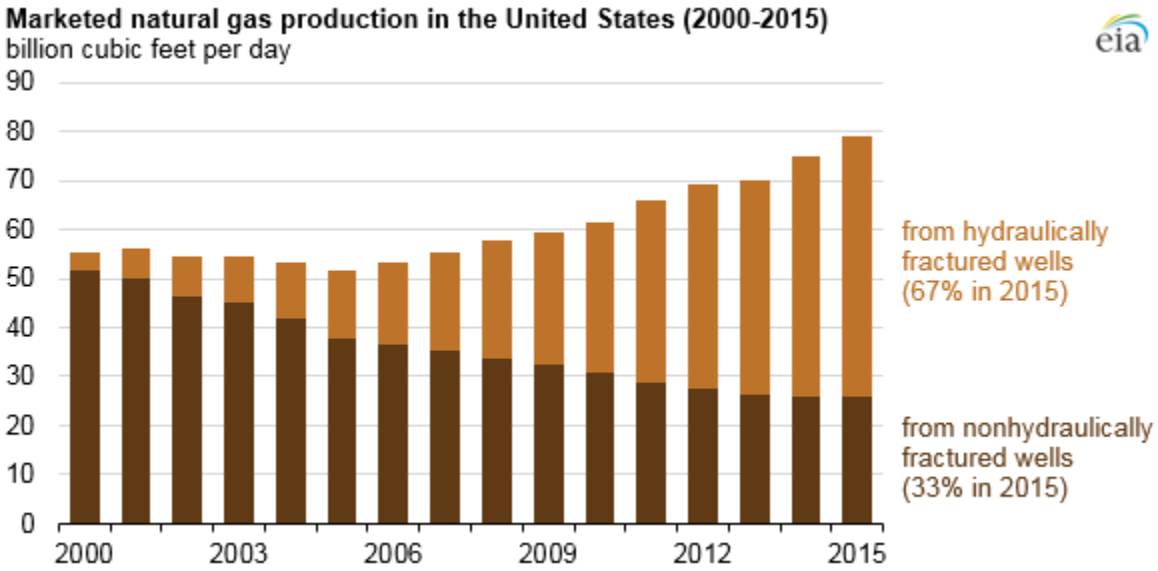

Figure 1.3: U.S. natural gas production from hydraulically fractured wells and from non-hydraulically fractured wells (2000-2015) (U.S. Energy Information Administration, IHS Global Insight, and DrillingInfo, 2016). (https://www.eia.gov/todayinenergy/detail.php?id=26112)

To better design hydraulic fracturing jobs, engineers need to predict fracture geometries based on formation geomechical properties and operation parameters. Fracture width and proppant distribution are crucial to fracture conductivity in production. Fracture spacing, length and height determine facture contact area with the formation (Fisher and Warpinski, 2012). Fracture contact area and fracture conductivity together decide if a fracturing job is successful.

Sequential and simultaneous fracturing methods are widely used in hydraulically fractured horizontal wells. Fracture spacing is the separation between adjacent open fractures. To effectively produce the reservoir, fracture spacing is usually minimized to improve drainage. However, interaction between simultaneous fractures causes fractures to propagate in complex patterns when fractures are close (Olson and Wu, 2012; Wu and

Olson, 2015). Optimizing fracture spacing requires increasing number of fracturing cluster and evenly stimulating each cluster.

Among the concerning factors, fracture height growth and containment is increasingly drawing researchers' attention since it controls fracture area within the pay zone. Unnecessary fracturing fluid, proppant and pumping horsepower is reduced by avoiding fracturing into upper and lower layers, which ultimately affects cost efficiency of fracturing jobs. In addition, operating within the target layer is a top concern for fracturing operations in some shallow reservoirs due to environmental concerns. Shale formations are mostly made of laminated layers of different mineralogy. In-situ stresses between layers are usually not uniform, and the magnitude of the difference may affect hydraulic fracture propagation and height growth. Understanding fracture height growth is especially important in multi-play development such as stack and staggered well pad designs (Figure 1.4).

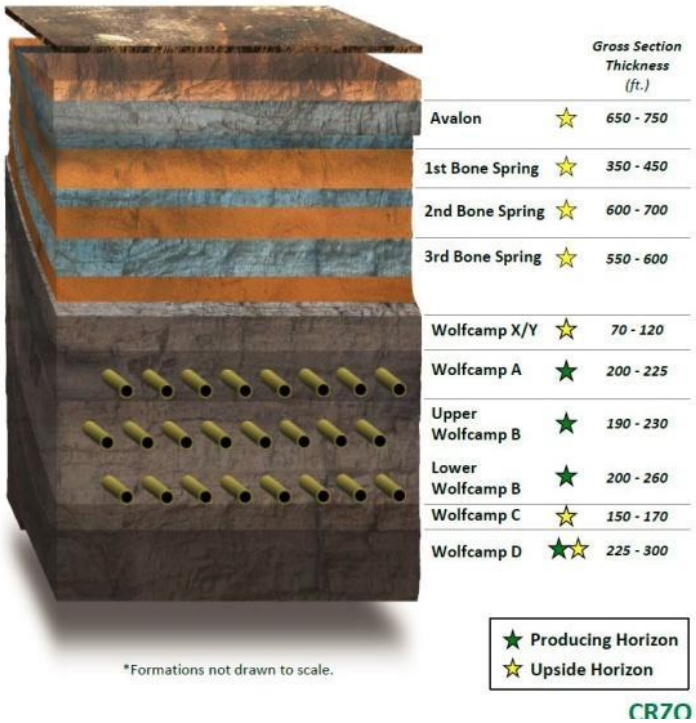

Figure 1.4: Multi-play development plan from one of the unconventional operators in Delaware basin (Carrizo Oil & Gas investor relation presentation, 2017)

1.2 RESEARCH OBJECTIVE

The objective of the thesis is to develop a computationally efficient hydraulic fracture model that incorporates fracture height growth determination in layered formation. The application of the model is to provide knowledge on fracture geometry optimization for field operations.

This thesis approached the primary objective in two steps, which is organized into two chapters:

i. Derive two novel correction factors to improve the simplified 3D DDM method (Wu and Olson, 2015) for fractures of non-uniform height in formations with

layered stress while still preserving the computational efficiency of the original method.

ii. Construct a physical methodology to calculate fracture height growth rate and apply the height growth methodology in multi-fracture propagation model based on the improved simplified 3D DDM method to predict fracture geometry.

1.3 LITERATURE REVIEW

We review the existing scientific literatures on fracture propagation models with a focus on the simplified 3S DDM method, unconventional layered formation geomechanical properties and fracture height containment theories.

1.3.1 Fracture Propagation Models

Since the 1950's, hydraulic fracture propagation models have been evolving from conventional two-dimensional single-fracture models, including well-known radial (or penny-shaled) fracture model (Sneddon, 1946 and Green and Sneddon, 1950; Segedin, 1951), the Khristianovich-Geertsma-DeKlerk (KGD) model (Khristianovich and Zheltov, 1955; Geertsma and de Klerk, 1969) and the Perkins-Kern-Norgren (PKN) model (Perkins and Kern, 1961; Nordgren, 1972), to pseudo three-dimensional models and fully three-dimensional models. Motivated by the recent shale boom in the petroleum industry and accessible high-powered computers, various complex muli-fracture models have been developed to simulate fractures generated by hydraulic stimulations in shale formations.

The conventional two-dimensional fracture models are simple in terms of calculation and can be used in certain well-studied formations. Generally two-dimensional fracture models fix one dimension which is normally fracture height, and calculate the

other two dimensions. Radial fracture model fixes the fracture height at wellbore to be twice of fracture radius (R) (Figure 1.5). The aperture of a penny-shaped fracture at distance r from the fracture initiation point is given as (Sneddon, 1946 and Green and Sneddon, 1950; Segedin, 1951):

$$D_n(r) = \frac{4(1-\nu)PR}{\pi G}\sqrt{1-(\frac{r}{R})^2}\ , \tag{1.1}$$

where v is Poisson's ratio, P is the pressure inside the fracture, R is fracture radius and G is the shear modulus. The radial fracture model is appropriate for the fracture initiation process (Peirce and Bunger, 2015) and small treatments in formations with thick pay.

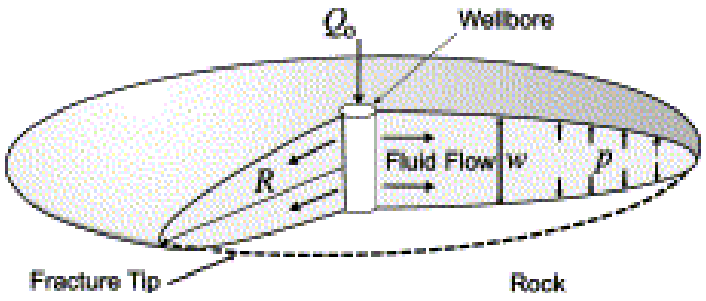

Figure 1.5: Schematic view of a radial or penny-shaped fracture initiated from a vertical wellbore (from Savitski and Detournay, 2002)

Both the KGD and PKN models assume plain strain deformation and calculate fracture width based on analytical solutions from elastic mechanics:

$$w(x,z,t) = \frac{(1-\nu)R}{G}(h^2 - 4z^2)^{1/2} P_{net}(x,t), \quad (1.2)$$

where w is the fracture width, v is Poisson's ratio, P_{net} is the net pressure inside the fracture, h is fracture height and G is the shear modulus. Fracture height is usually assumed to be the same as layer thickness. KGD and PKN models differ primarily because they assume plain strain in different directions.

The KGD model (Figure 1.6) assumes plane strain in the horizontal plane and a rectangular cross-section in vertical direction. The fluid flow equation for flow in a rectangular slot is applied to calculate pressure drop from wellbore to fracture tip,

$$q = -\frac{w^3 h}{12\mu}\frac{dp}{dx}, \quad (1.2)$$

where q is the fluid injection rate, w is the fracture width, μ is fluid viscosity, P is the effective pressure on fracture surface, h is fracture height. The KGD model assumes the fracture height is much longer than fracture length and is suitable for short-length fractures, such as fracture propagation at early stage of injection. On the other hand, the PKN model (Figure 1.7) assumes plane stain in the vertical direction and fracture width varies in the vertical direction following an elliptical shape. The fluid flow equation for flow in a fracture with elliptical cross-section is applied,

$$q = -\frac{\pi w_{\max}{}^3 h}{64\mu}\frac{dp}{dx}, \quad (1.3)$$

where w_{max} is the maximum fracture width at vertical center. The PKN model is commonly used when fracture length is much larger than height, which is the case at late injection time.

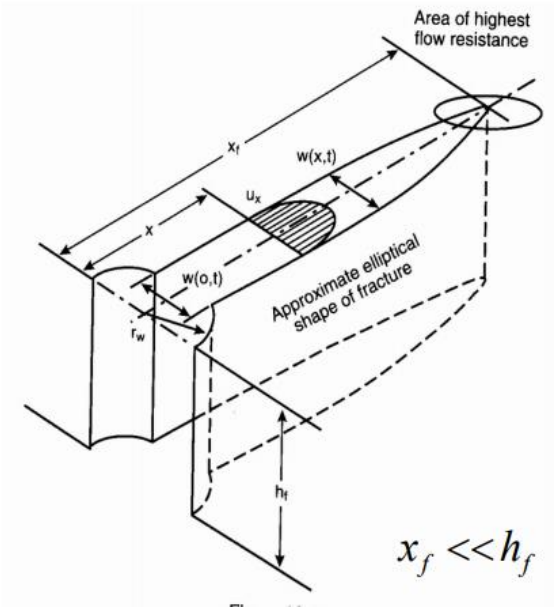

Figure 1.6: Schematic view of a KGD fracture model (from Geertsma and de Klerk, 1969)

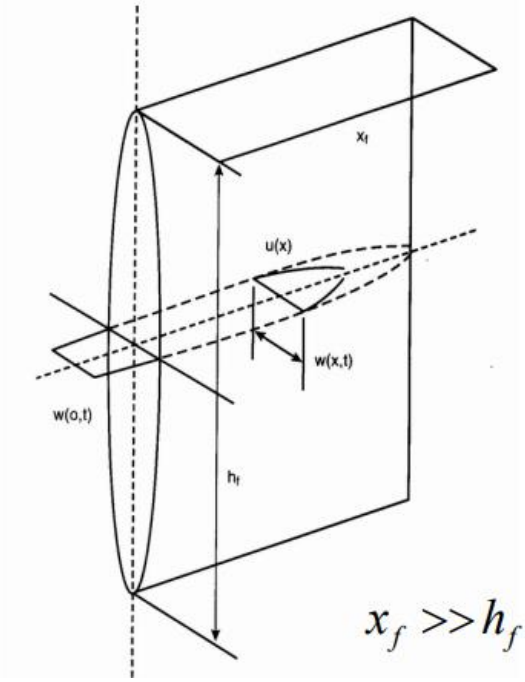

Figure 1.7: Schematic view of a PKN fracture model (from Nordgren et al., 1972)

The two-dimensional models mentioned above provide great validation points for developing complicated fracture models. A constant height model is applicable in a layered sequence where the barriers are extremely effective and don't allow height growth. These models require the height to be assumed, and height is often unknown. To predict the growth of a single fracture through layers with different confining stress, Simonson et al. (1978) developed a height growth solution for fractures in a symmetric three-layer formation with different in-situ stresses, and taken into account of pressure gradient over fracture height. Fung et al. (1987) extended Simonson et al.'s solution to asymmetric multi-layer cases. Pseudo-3D models were developed by implementing the height growth solution and most of the models assume fluid flow is 1D along fracture length direction (Valko and Economides, 1995). Pseudo-3D models are effective attempts to capture the physical behavior of single fracture propagation incorporating height growth. Some of the commercial hydraulic fracturing simulators today are still constructed based on pseudo-3D fracture models.

True 3D single planar-fracture models attempt to couple three-dimensional rock deformation and two-dimensional or three-dimensional fluid flow in the fracture. The computational power requirement to run the fully-3D models are achievable though high efficacy computers but the model run-time is still long.

Recent successful unconventional reservoir development is associated with completion strategy of multi-frac simultaneous stimulation (Figure 1.8). Plug-n-perf is a common field practice to generate multiple fractures simultaneously. The wellbore is isolated into up to hundreds of frac stages, and each stage interval is perforated with several clusters as fluid entry points for fracture initiation. Modeling multi-frac propagation is different from conventional single fracture model with two new problems to solve,

mechanical interaction between fractures and fluid flow distribution in wellbore and among fractures.

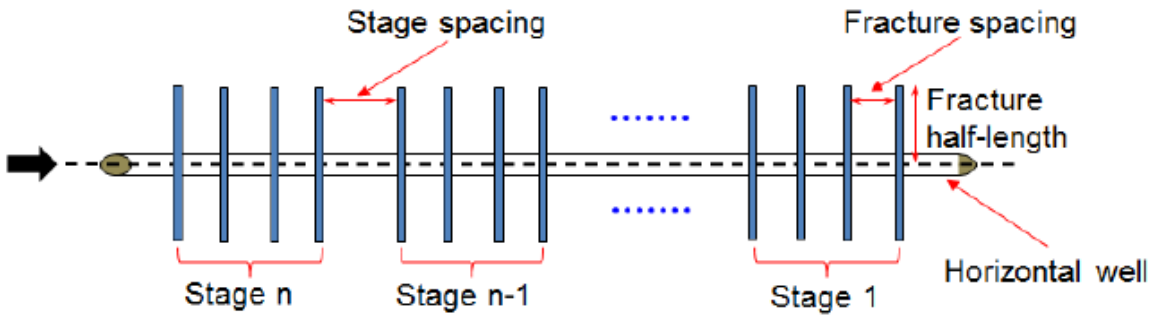

Figure 1.8: Illustration of multiple hydraulic fracturing design (from Wu, 2014)

Mechanical interaction between fractures or the stress-shadow effect is one of the main causes of non-planar fracture propagation and un-even fracture development initiated from different clusters within a frac stage. Fracture interaction could be solved by analytical solutions (Sneddon and Elliot, 1946) and numerical methods. The numerical method mainly includes three types, displacement discontinuity method (Shou et al., 1993; Olson et al., 2009; Cheng, 2009; Wu and Olson, 2015), finite difference method (Roussel and Sharma, 2011) and finite element method (Shin and Sharma, 2014). The common practice for calculating fluid distribution among fractures and wellbore is to use an electrical current analogue (Elbel et al., 1992; Mack et al., 1992; Yi and Sharma, 2018). Several recent multi-frac propagation models are developed with iteratively coupled rock deformation and fluid flow solutions (Xu and Wong, 2013; Shin and Sharma, 2014; Wu and Olson, 2015; McClure and Kang, 2017). Wu and Olson (2015) modeled multiple fracture propagation in horizontal wells by coupling a novel simplified 3D displacement discontinuity method to calculate rock deformation with a fluid flow model, which greatly

improved the computational efficiency of the model while preserving the accuracy of a fully 3D model.

1.3.2 Unconventional Layered Formation

Layered sedimentary formations or stratigraphic succession in geological terms is formed by fluctuation of water level, for example sea level (Nichols, 2009). Different energy and depositional facies in the fluctuation cycles determine the rock type and mechanical properties in a layer. The transgression and regression cycles of sea level causes the vertical stratigraphic succession (Nichols, 2009). For example, the Eagle Ford shale was deposited in an overall sea level regression with a series of higher frequency transgressive-regressive cycles within the formation (Ferrill et al., 2014). This caused the alternation of fine-grain mudstone and coarse-grain chalk (Workman, 2013).

Usually unconventional formations are made of laminated layers of different mineralogy. The scale of lamination is different for different reservoirs. For the Mesaverde reservoir in Green River basin of Wyoming, thin beds of less than an inch (Figure 1.9) are observed in an eight-inch core (Miskimins and Barree, 2003). In the outcrops of Eagle Ford formation in Sycamore Creek pavement, mudstone and chalk beds are around half of a foot in thickness (Ferrill et al., 2014).

Figure 1.9: Left: 8-inch core section from the Mesacerde reservoir. Thin bedded sand in light gray and shale in dark gray can be observed in the scale of half-inch (from Miskimins, 2003). Right: succession of chalk and mudstone in the outcrops of Eagle Ford formation. The layer thickness is slightly less than a foot (from Ferrill et al., 2014)

1.3.3 Fracture Height Containment Mechanism

In layered formations, fractures demonstrate four types of behavior when reaching vertical layer interfaces as shown in Figure 1.10 (Thiercelin et al., 1987). As two extreme cases, fractures could penetrate the bedding planes or get arrested by the interface. In other more complex cases, fractures may be deflected by the interface or sometimes reinitiate into adjacent layer at some point along the interface. Fracture height containment depends on the fracture growth pattern at layer interface, and fracture complexity is challenging for proppant transport. Therefore it is important to determine which behavior fractures will follow at the interface, given certain layer properties. All those behaviors have been observed in laboratory experiments, but most 3D hydraulic fracturing simulators could only model the two extreme cases.

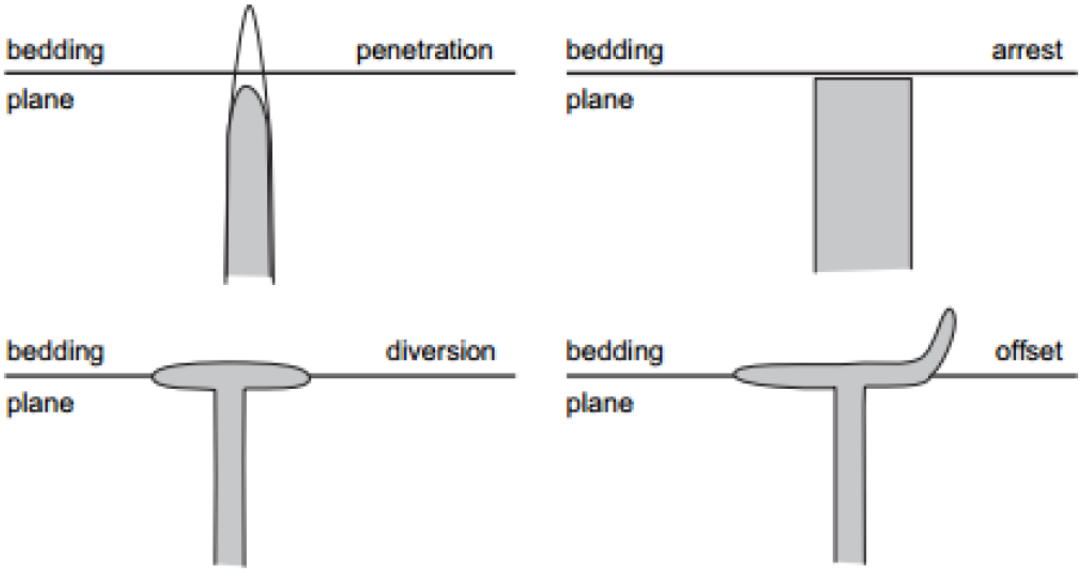

Figure 1.10: Four types of behavior when fractures reach layer interfaces (from Thiercelin et al., 1987)

Numerous research on fracture height containment mechanisms have been conducted through extensive laboratory and simulation studies. The results indicate fracture height containment is mainly controlled by in-situ stress contrast, mechanical property heterogeneity and weak interface between layers in terms of formation property. Operation parameters such as fluid viscosity and treating pressure also affect fracture height growth.

In layered formations, fracture height containment due to in-situ stress contrast between layers is most common and well-studied (Warpinski et al. 1994). An upper limit for fracture height could be calculated using equilibrium height models due to in-situ stress contrast. Equilibrium height is determined by setting the stress intensity factor K_I, equal to fracture toughness K_{IC}. The stress intensity factor is calculated by integration of net pressure along fracture height through all the layers. The first equilibrium model

considered three layer cases with upper layer, target layer and lower layer (Simonson et al., 1978) and several models have been developed later to investigate more complicated cases with nonsymmetrical fracture height growth (Economides et al., 2012) and greater than three stress layers (Liu and Valko, 2015; Fung et al. 1987; Economides and Nolte, 2000). Note that the in-situ stress contrast only serves as a fracture height barrier when there is higher stress in the confining layers than in the pay or treatment zone.

The change of mechanical properties such as Young's modulus and Poisson's ratio between layers affects fracture height growth in indirect ways. The stress intensity factor at vertical tips is lowered when the fracture grow into a stiffer layer (Simonson et al., 1978), which could cause the fractures to stop at the boundary. Meanwhile, fracture width and internal pressure is affected when it penetrate into a stiffer or softer layer. Van Eekelen (1982) suggests the reduction on fluid flow rate in stiffer layers could hinder fracture height growth. Gu and Siebrits (2008), on the other hand, suggest the effect of layer modulus difference on fracture height also depends on the tip location. Yue et al. (2018) studied the impact of modulus values, fracture tip location and height percentage of rock layers on calculating effective modulus of a layered reservoir.

Mechanical property contrast is also the potential cause of in-situ stress difference. As in-situ stress measurements of formation layers are not always available, it is possible to reconstruct the in-situ stress profile in the formation with mechanical properties and predict fracture height growth. Blanton and Olson (1997) estimated in-situ stresses from logs based on overburden, Poisson's ratio, pore pressure effects, temperature and tectonics.

1.4 THESIS ORGANIZATION

The thesis is organized into four chapters. Chapter 1 introduces the scope and objective of this research project and a literature review on related topics. Chapter 2

provides details of the improved simplified 3D model and validation results from static fracture simulations. In Chapter 3, a novel height growth methodology is introduced and the improved model developed in Chapter 2 is applied to simulate fracture propagation and height growth in layered formation. Chapter 4 presents conclusions from current research and gives recommendations for future research.

Chapter 2: Improvements on Simplified Three-Dimensional Displacement Discontinuity Method to Model Fracture in Layered Formations[1]

In this chapter, an improved version of the Simplified 3D Displacement Discontinuity Method (S3D DDM) is introduced which can be used to simulate single and multiple fracture problems in a layered formation. The developed model is then used to predict the geometry of hydraulic fractures, and to characterize the stress shadowing effect between fractures with variable heights and vertical offsets.

Similar to the original S3D DDM, 3D correction factors are used to calculate the normal and shear displacements along the fracture length. For this improved version, the original 3D correction factors are modified to account for fractures with non-uniform height along the length direction. A stress correction factor is employed to calculate the influence of stress contrast between layers on fracture opening. Static simulation results from the improved model compare favorably with reference analytical solutions for penny-shaped fractures and with fully 3D numerical solutions. While the fully 3D model requires discretization in both lateral and vertical directions, the simplified model requires only a single row of elements in height, resulting in considerably lower computation time and memory utilization with acceptable loss of accuracy.

[1] This chapter is based on join work with Omid Razavi, who contributed greatly to the literature review. Part of the chapter has been published in Li, T., Razavi, O. and Olson, J.E., 2018, August. Modeling Fracture in Layered Formations Using a Simplified 3D Displacement Discontinuity Method. In 52nd US Rock Mechanics/Geomechanics Symposium. American Rock Mechanics Association.

2.1 INTRODUCTION

Microseismic observations and other field data suggest that hydraulic fractures are often not contained within a single layer (Fisher and Warpinski, 2012). Acoustic log data show that rock mechanical properties typically vary significantly between layers, leading to confining stress contrasts across bedding planes (Teufel and Warpinski, 1983). Simulating the propagation of multiple hydraulic fractures in such a multi-layer environment represents a unique challenge when trying to achieve both numerical efficiency and accuracy.

Many analytical and numerical solutions exist to solve fracture problems in homogeneous formations (SNEDDON, 1946; Pollard and Segall, 1987; Warpinski et al., 1994; Weng et al., 2011; McClure, 2012; Dontsov and Peirce, 2015; Wu and Olson, 2015). The Displacement Discontinuity Method (DDM) seems a particularly suitable approach for fracture propagation given its superior accuracy and simplicity to predict multiple fracture propagation path. However, a fully 3D DDM simulation can be computationally expensive for multiple hydraulic fractures applications.

In an effort to reduce the computational cost of hydraulic fracturing simulations, Wu and Olson (2015) proposed a Simplified 3D (S3D) DDM for multiple fracture propagation problem, assuming fractures of constant height contained within a single layer. This method reduces computational cost by requiring fractures to have a vertical dip (all dip-slip equations are removed from the calculation) and using only a single row of elements along the fracture height. Accuracy is achieved with this simplified method through the use of semi-empirical correction factors that depend on fracture geometry and spacing (Wu and Olson, 2015). In this chapter, this simplified method is extended to a more general case. New 3D corrections factors are developed to account for non-uniform fracture height along the length direction and for fractures to span multiple stress layers.

Static simulation results from the improved model are validated against a reference analytical solution for penny-shaped fractures and a fully 3D DDM numerical solution.

2.3 3D CORRECTION FACTORS

Wu and Olson (2015) modified the 3D displacement discontinuity method equations of Shou (1993), deriving the following new equations for normal and shear stresses, σ_{ij}, induced by displacement discontinuity elements (Figure 2.1) as:

$$\begin{aligned}
\sigma_{11} &= C_{11}C_r D_1[2I_{,11} - x_3 I_{,111}] + C_{11}C_r D_3[I_{,33} + (1-2\nu)I_{,22} - x_3 I_{,311}] \\
\sigma_{33} &= C_{11}C_r D_1[-x_3 I_{,133}] + C_{11}C_r D_3[I_{,33} - x_3 I_{,333}] \\
\sigma_{22} &= C_{11}C_r D_1[2\nu I_{,13} - x_3 I_{,122}] + C_{11}C_r D_3[I_{,33} + (1-2\nu)I_{,11} - x_3 I_{,322}] \\
\sigma_{13} &= C_{13}C_r D_1[I_{,33} + \nu I_{,22} - x_3 I_{,113}] + C_{13}C_r D_3[-x_3 I_{,313}] \\
\sigma_{21} &= C_r D_1[(1-\nu)I_{,23} - x_3 I_{,112}] + C_r D_3[-(1-2\nu)I_{,12} - x_3 I_{,312}] \\
\sigma_{23} &= C_r D_1[-\nu I_{,21} - x_3 I_{,123}] + C_r D_3[-x_3 I_{,323}]
\end{aligned}, \quad (2.1)$$

in which, x_i is the right-handed coordinate system where x_2 is vertical, D_1 and D_3 are the normal and strike-slip shear displacement discontinuity, respectively, ν is Poisson's ratio, C_{ij} are the algebraic correction factors, and

$$C_r = \frac{\mu}{4\pi(1-\nu)}. \quad (2.2)$$

The kernel analytical solution of I was proposed by Crouch and Starfield (1983),

$$I(x_1, x_2, x_3) = [\bar{x}_1 \ln(r + \bar{x}_2) + \bar{x}_2 \ln(r + \bar{x}_1) - x_3\theta]\Big|_{\substack{\xi_1=a \\ \xi_1=-a}}^{\xi_2=b} \Big|_{\xi_2=-b}. \quad (2.3)$$

In which,

$$\bar{x}_1 = x_1 - \xi_1,$$
$$\bar{x}_2 = x_2 - \xi_2,$$
$$\theta = \tan^{-1}[\bar{x}_1 \bar{x}_2 / (r x_3)]' \quad .$$
$$r = \sqrt{(x_1 - \xi_1)^2 + (x_2 - \xi_2)^2 + x_3^2}.$$

and the partial derivatives of I with respect to x_i ($I_{,i}$, $I_{,ii}$, and $I_{,iii}$) were derived by Shou (1993).

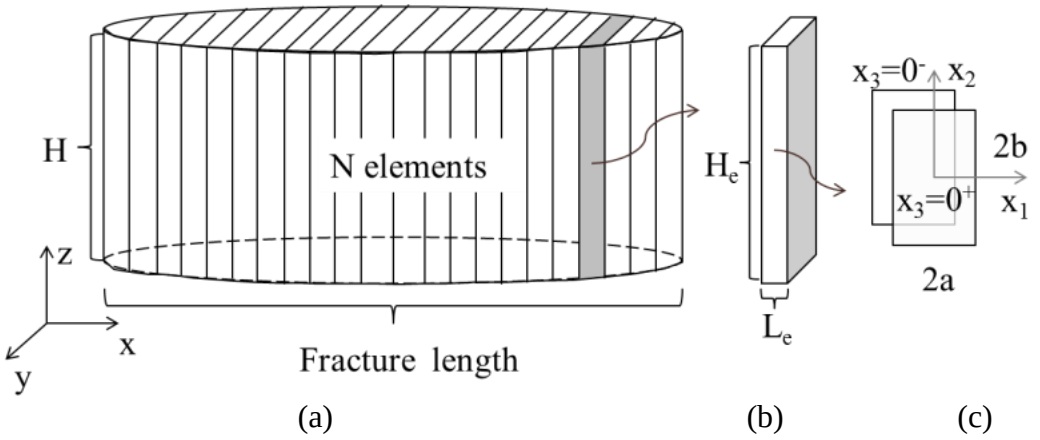

Figure 2.1: (a) A 3D fracture discretized in x direction in an infinite elastic media adapted from Wu and Olson (2015); (b) One fracture element of height He and length Le; (c) Local coordinates of the element.

Wu and Olson (2015) reformulated the stress equations based on analytical solutions (Rongved, 1957; Salamon, 1964) with a few simplifications and assumptions. In the subsurface, the vertical stress is a principal stress and is typically larger than the minimum horizontal stress. Under these conditions, hydraulic fractures are most likely to have a vertical or near vertical dip and are unlikely to have dip-slip mode shearing. Eliminating one direction of shearing is helpful computationally because it eliminates one unknown, the displacement discontinuity in the dip-slip direction, D_2. The 3D correction factors C_{11} and C_{13} are added to the stress equations to compensate for lack of discretization

in vertical direction. In the previous S3D method (Wu and Olson, 2015), the correction factors were derived from the analytical solution for normal and shear stresses (Rongved, 1957; Salamon, 1964) as:

$$\begin{aligned} C_{11} &= 1 - \frac{d^{\beta_1}(H/\alpha)^{\beta_2}}{(d^2+(H/\alpha)^2)^{(\beta_1+\beta_2)/2}},\ (\beta_1 = 1.5\ \ \beta_2 = 4\ \ \alpha = 1) \\ C_{13} &= 1 - \frac{d^{\beta_1}(H/\alpha)^{\beta_2}}{(d^2+(H/\alpha)^2)^{(\beta_1+\beta_2)/2}},\ (\beta_1 = 1.8\ \ \beta_2 = 4\ \ \alpha = 1) \end{aligned}, \tag{2.4}$$

where H is the fracture height (presumed equal to layer thickness) and d is the distance between the centers of elements.

The newly derived correction factors shown in equation (2.5) relax the requirement of uniform fracture height among elements by incorporating a term based on the element aspect ratio L_e/H_e (Figure 2.2) described in equation (2.6). In this function, c and β_3 are empirically determined constants.

$$\begin{aligned} C_{11} &= 1 - \frac{d^{\beta_1}(H_e \times f(L_e/H_e)/\alpha)^{\beta_2}}{(d^2+(H_e/\alpha)^2)^{(\beta_1+\beta_2)/2}},\ (\beta_1 = 1.5\ \ \beta_2 = 4\ \ \alpha = 1) \\ C_{13} &= 1 - \frac{d^{\beta_1}(H_e \times f(L_e/H_e)/\alpha)^{\beta_2}}{(d^2+(H_e/\alpha)^2)^{(\beta_1+\beta_2)/2}},\ (\beta_1 = 1.8\ \ \beta_2 = 4\ \ \alpha = 1) \end{aligned}, \tag{2.5}$$

in which

$$f(L_e/H_e) = c^{(L_e/H_e - \beta_3)}\ \ (c = 1.6\ \ \beta_3 = 0.1). \tag{2.6}$$

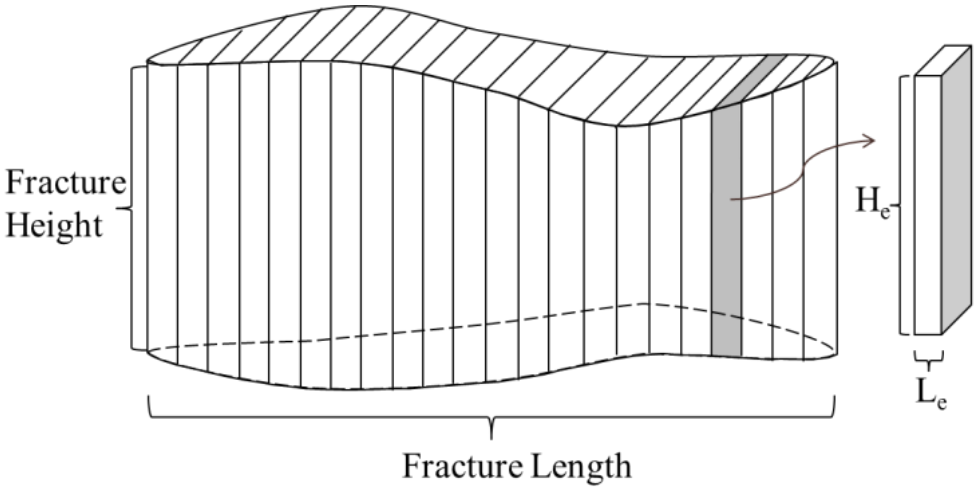

Figure 2.2: (a) 3D fracture profile with non-uniform height in length direction; (b) one fracture element of height H_e and length L_e.

2.4 STRESS CORRECTION FACTOR

In order to apply the S3D DDM method to reservoirs layered in stress (Figure 2.3), the stress displacement equations are further modified to reflect stress contrast between formation layers. Mechanical properties are still assumed to be homogeneous, but we anticipate incorporating modulus heterogeneity in future work. The effective net pressure for each fracture element is calculated as:

$$\overline{P_{net}} = P_f - F\sigma_n, \tag{2.7}$$

where P_f is the fluid pressure inside the fracture and σ_n is the normal stress acting on fracture surface at perforation depth. A stress correction factor F is applied in equation (2.7) to account for changing of differences in the normal stress between the perforated zone and the layers above and below. The effective net pressure is the net normal stress applied on the fracture surface and directly determines the local stress field (σ_{ii}) of a fracture element

after coordinate transformation (Wu and Olson, 2015). The normal and shear displacement discontinuities are calculated by equation 2.1.

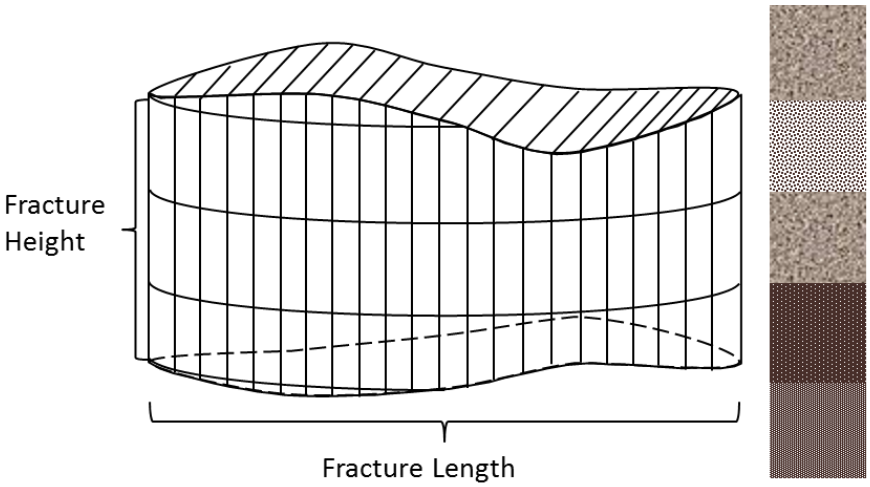

(a)

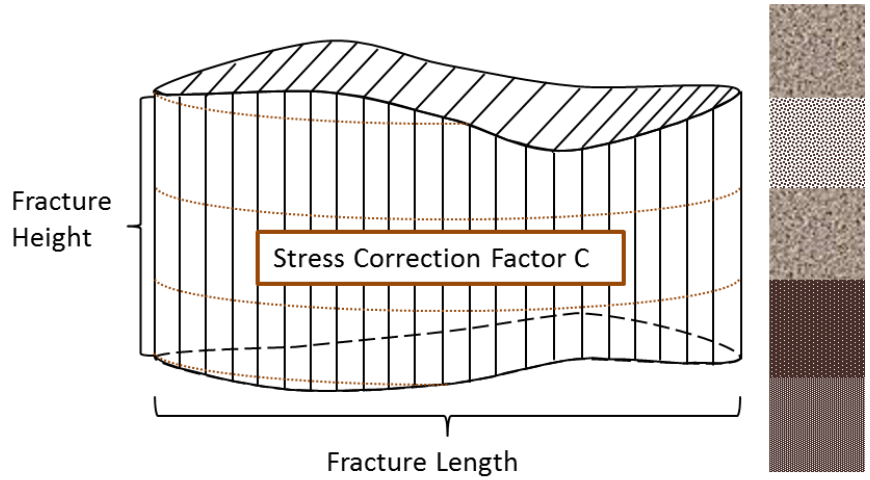

(b)

Figure 2.3: (a) Standard 3D method discretizes elements vertically at least for each layer (solid lines), which requires re-mesh for dynamic fractures. (b) The improved S3D method implements a stress correction factor to account for the in-situ stress difference in layers. Only one row of elements in height direction is utilized and the dashed lines are not discretization.

The stress correction factor, *F*, is modeled after the plane strain equation for fracture opening derived by Nolte and Economides (2000) given by

$$w(z) = \frac{4}{E'}[P_{cp} - \sigma_n + \rho_f g(h_{cp} - \frac{h}{4} - \frac{z}{2})]\sqrt{z(h-z)} + \frac{4}{\pi E'}\sum_{i=1}^{n-1}(\sigma_{i+1} - \sigma_i)[(h_i - z)\cosh^{-1}\frac{z(\frac{h-2h_i}{h}) + h_i}{|z - h_i|} + \sqrt{z(h-z)}\arccos(\frac{h-2h_i}{h})] \quad (2.8)$$

In equation (2.8), *E'* is the plane strain modulus which is assumed to be constant in this study and $E' = E/(1-\nu^2)$, *h* is the total height of the fracture, h_i is the height from fracture bottom tip to the top of layer *i*, P_{cp} and σ_n are the net pressure and normal stress at perforation position h_{cp}, σ_i is the normal stress acting on the fracture in layer *i*, and ρ_f is the fracturing fluid density. The determining factors in this analytical equation are difference of normal stress σ_i between layers, the layer height h_i and the relative location of the evaluation point, *z*, compared to fracture height, *h*. Considering all the key elements in determining the fracture width profile, the stress correction *F* for a layered formation has been determined as,

$$F = 1 + \sum_{i=1}^{n}\frac{\sigma_i - \sigma_{perf}}{\sigma_{perf}}\frac{[z_i(h-z_i)]^b}{h^{2b}}(\frac{h_i}{h})^a \ , (a = 1.2 \quad b = 0.2), \quad (2.9)$$

where z_i is the height at the center of layer i, measured from fracture bottom tip (Figure 2.4), and *a* and *b* are empirically derived coefficients. Figure 2.4 shows the 3D and side view of a vertical hydraulic fracture that grows into the upper and lower layers from the perforation layer. The fracture is perforated at layer #2 and so $\sigma_{perf} = \sigma_2$. Note that in order

to approach real formation condition, the correction factor is not limited to the three layers case and can accommodate an asymmetric normal stress profile.

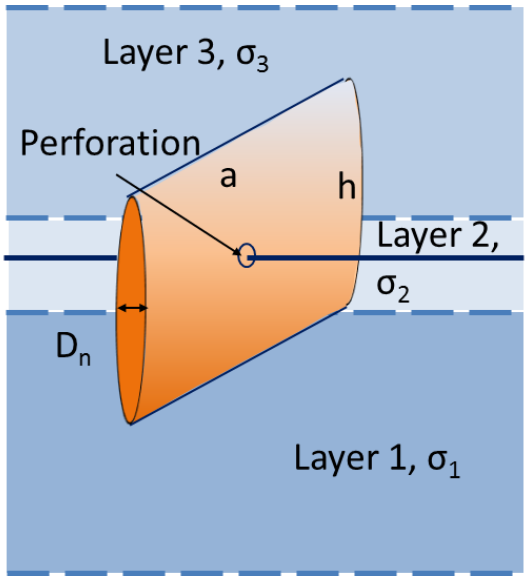

(a)

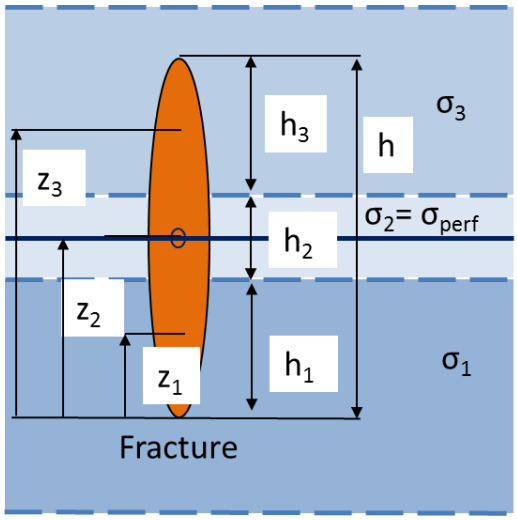

(b)

Figure 2.4: (a) 3D view of the single fracture; (b) the side view of the same fracture with properties labeled.

2.5 VALIDATION

In order to validate the improved S3D DDM, static simulation results were compared with analytical solutions or the fully 3D equations of Shou (1993). We also included a comparison with the previous method of Wu and Olson (2015) to show the effect of non-uniform height and layered stress on that solution.

2.5.1 Single Fracture with Non-uniform Height

A penny-shaped fracture geometry was chosen to examine the accuracy of the improved method on handling non-uniform height (Figure 2.5). The model still uses one row of elements, while the element aspect ratio L_e/H_e is varying based on the shape function. Since the validation is performed on a static fracture condition, the net pressure is assumed to be 300 psi uniformly distributed in the fracture, and the fracture radius (R) is fixed at 100 ft (Table 2.1). Simulation results are compared with the analytical solution for a penny shaped fracture (Sneddon, 1946 and Green and Sneddon, 1950; Segedin, 1951). The normal displacement (D_n) at distance r from the initiation point is given as:

$$D_n(r) = \frac{4(1-\nu)P_{net}R}{\pi G}\sqrt{1-(\frac{r}{R})^2}\,, \tag{2.10}$$

where ν is Poisson's ratio, P_{net} is the net pressure inside the fracture, R is fracture radius and G is the shear modulus.

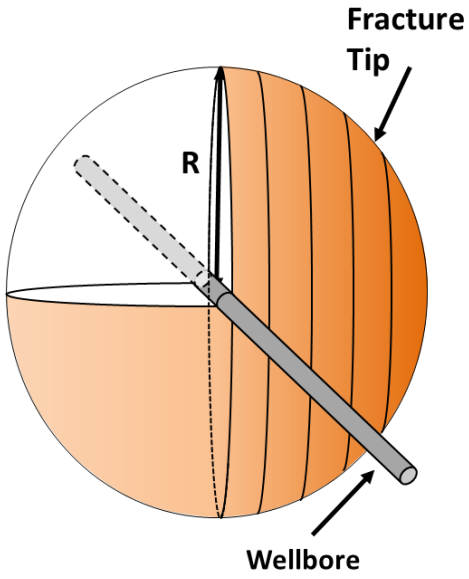

Figure 2.5: A vertical penny-shaped fracture with radius R initiated from a horizontal wellbore.

Fracture length or radius (R)	100 ft
Net pressure (P_{net})	300 psi
Young's Modulus (E)	4×10^6 psi
Poison's ratio (v)	0.25

Table 2.1: Input parameters for penny-shaped fracture case.

For the improved S3D method, the fracture is discretized into 60 elements along length direction. There was no discretization in the height direction, such that there was only one row of elements. The same input parameters were used to run the S3D model. Normal displacement discontinuities (D_n) at different points of fracture length for the penny-shaped fracture are plotted in Figure 2.6, along with the analytical reference results. A very close match was observed between the improved S3D method and the

analytical solution. Fracture aperture results are also plotted against fracture element aspect ratio in Figure 2.7 for both methods. Both results show that the improved S3D method accurately predicts fracture aperture using various element aspect ratios.

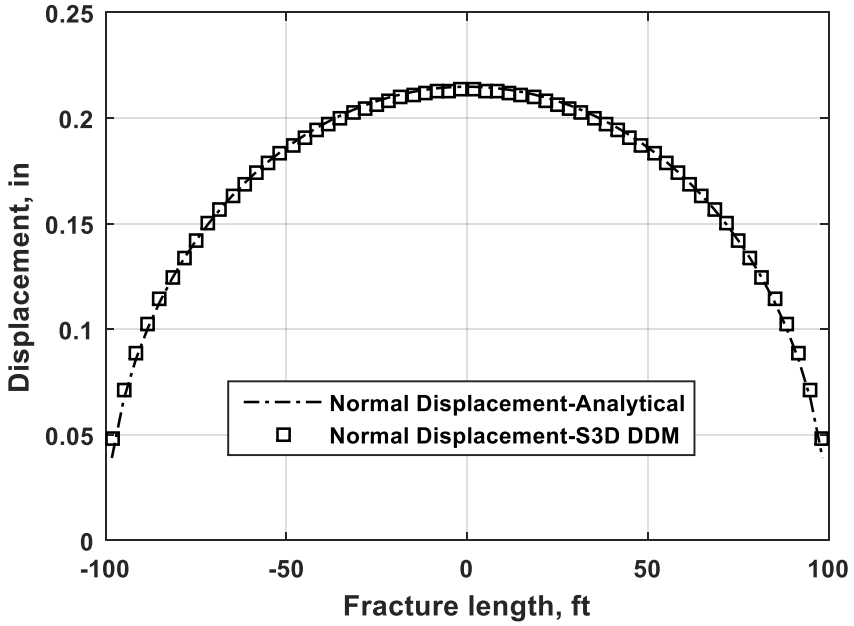

Figure 2.6: Normal displacement discontinuities or fracture aperture versus length for the penny-shaped fracture illustrated in Figure 2.5.

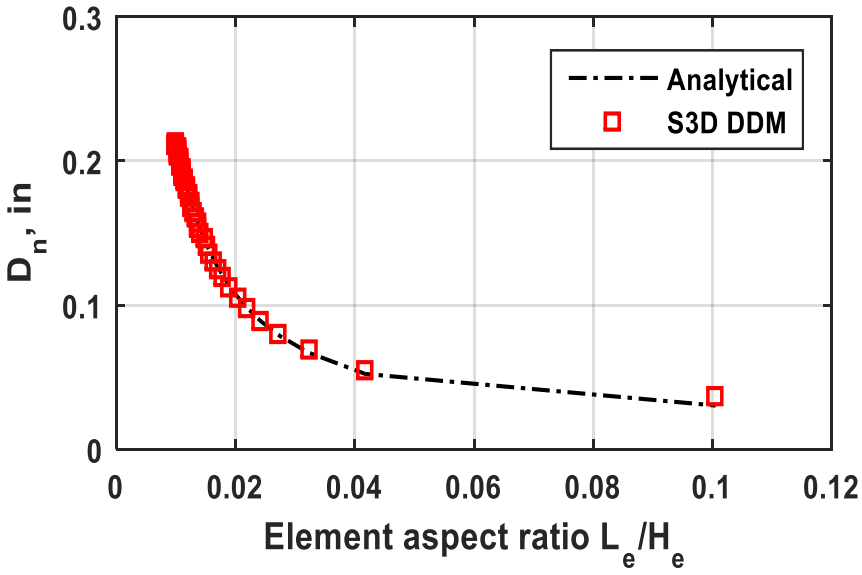

Figure 2.7: Fracture aperture plotted against element aspect ratio for the penny-shaped fracture.

2.5.2 Multiple Fractures within Single Layer

The accuracy of the improved 3D correction factor is further tested by comparing the predictions for the normal displacement discontinuities in multiple fracture cases. As discussed earlier, in the original version of the S3D DDM, it was assumed that the fractures are at the same depth. However, in the improved version, this restriction has been removed and the model may include fractures centered at different depths. Figure 2.8 shows two fractures within a distinct stress layer but at different depth. The net pressure inside the fractures is assumed to be equal. The horizontal spacing between the two fractures is set to be 100 ft, which is the same as the fracture height. Other input parameters are listed in Table 2.2.

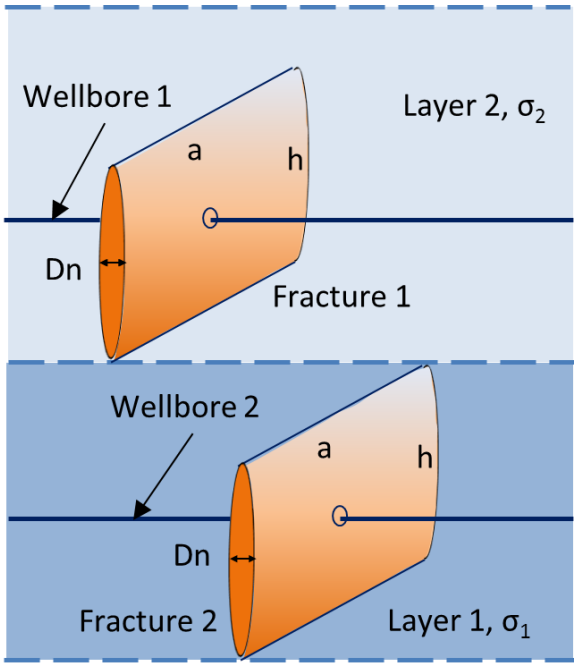

(a)

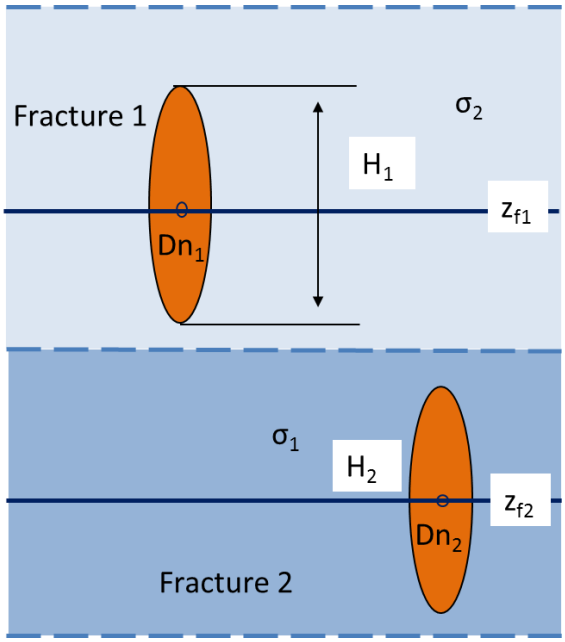

(b)

Figure 2.8: (a) 3D view of the two fractures; (b) side view of the same fractures. Fractures 1 and 2 are entirely within a uniform stress layer.

Fracture length for both fractures (L)	400 ft
Fracture height for both fractures (H)	100 ft
Horizontal spacing	100 ft
Vertical spacing	200 ft
Minimum horizontal stress in layer 1 (σ_1)	6000 psi
Minimum horizontal stress in layer 2 (σ_2)	5800 psi
Internal fluid pressure for both fractures (P_f)	6200 psi
Young's Modulus (E)	5×10^6 psi
Poison's ratio (v)	0.2

Table 2.2: Input parameters for the multi-fracture contained entirely within distinct stress layers case (show in Figure 2.8).

Figure 2.9 compares the aperture distribution calculated by the improved S3D method and the fully 3D DDM method (Shou, 1993). Good agreement is observed between the results for both fractures. Note that the fracture aperture of fracture #2 (red lines) is smaller than fracture #1 (black lines) due to the higher confining stress (+200 psi) in the lower layer. The obtained results indicate that the improved S3D method (which uses one row of elements for each fracture) yields the same level of accuracy as the fully 3D DDM (with 11 rows of elements).

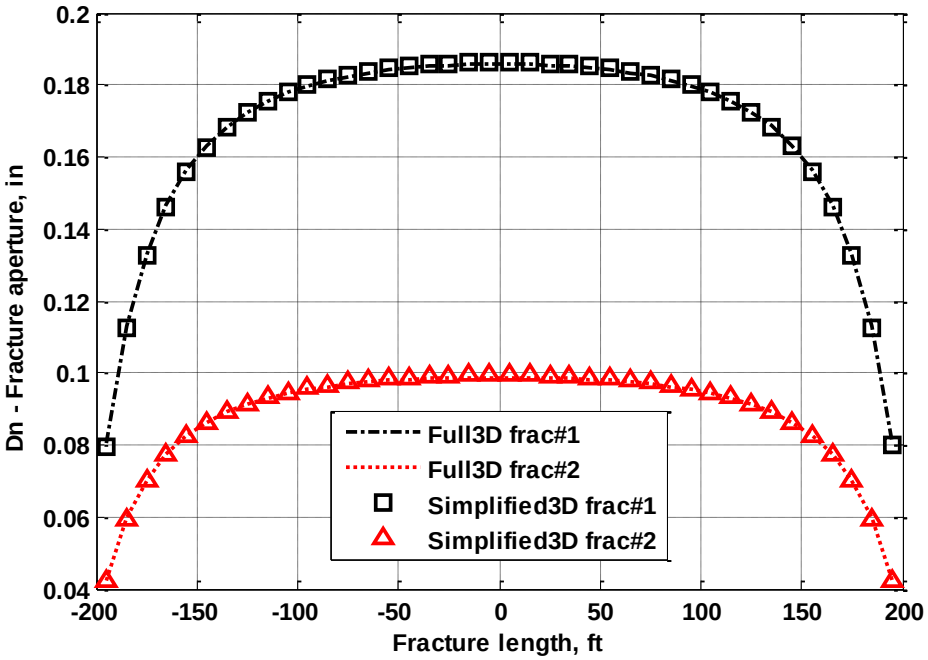

Figure 2.9: Fracture aperture versus length for the multi-fracture within single layer case.

2.5.3 Single Fracture in a Multi-layer Formation

In this section, the accuracy of the improved method to simulate a single fracture located at multiple stress layers is investigated. Figure 2.10 illustrates a single uniformly pressured fracture in a multi-layer formation. The in-situ stresses are heterogeneous in vertical direction, represented by different color scales. For this static model, the fracture penetrates layers adjacent to the perforation layer (layer #2). The stress contrast is 100 psi between layer #2 and #3 (top), and is 200 psi between layer #2 and #1 (bottom). Fracture length is 400 ft and fracture height is 100 ft. h_1, h_2 and h_3 represent the fracture height portions distributed in each layer. Table 2.3 presents the parameters used in the single fracture model shown in Figure 2.10.

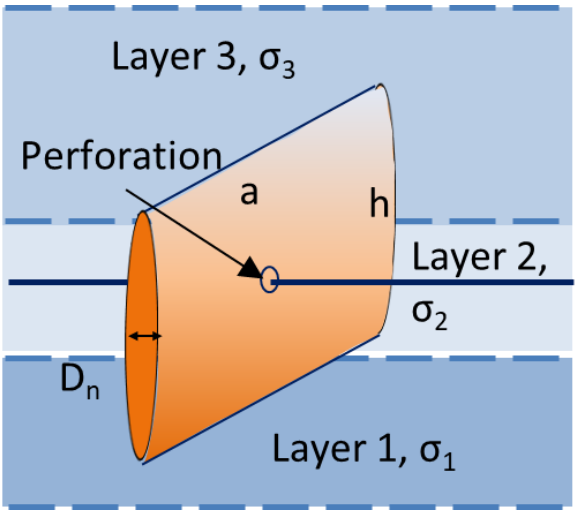

(a)

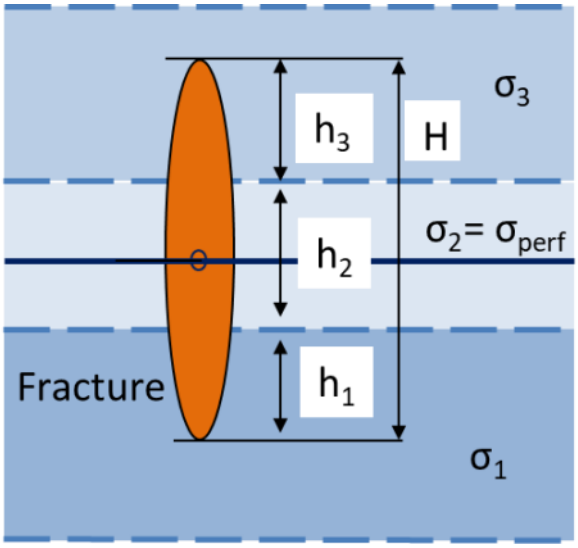

(b)

Figure 2.10: (a) 3D view; (b) side view of a single fracture in a multi-layer formation.

Fracture length for both fractures (L)	400 ft
Fracture height for both fractures (H)	100 ft
Minimum horizontal stress in layer 1 (σ_1)	6000 psi
Minimum horizontal stress in layer 2 (σ_2)	5800 psi
Minimum horizontal stress in layer 3 (σ_3)	5900 psi
Internal fluid pressure in for both fractures (P_f)	6200 psi
Young's Modulus (E)	5×10^6 psi
Poison's ratio (v)	0.2
h1, h2, h3	25, 50, 25 ft

Table 2.3: Input parameters for the single fracture in a multi-layer formation case (shown in Figure 10).

Simulations were performed using both the original S3D method and the improved S3D method, benchmarking them against the fully 3D results, to demonstrate the effect of the stress correction factor F. There is more than 20% difference in the fracture aperture estimate between the original S3D DDM results and the fully 3D DDM model (Figure 2.11a) for the layered stress case. The incorporation of the stress correction factor in the improved model, however (Figure 2.11b), results in a close match to the fully 3D result for the layered stress case.

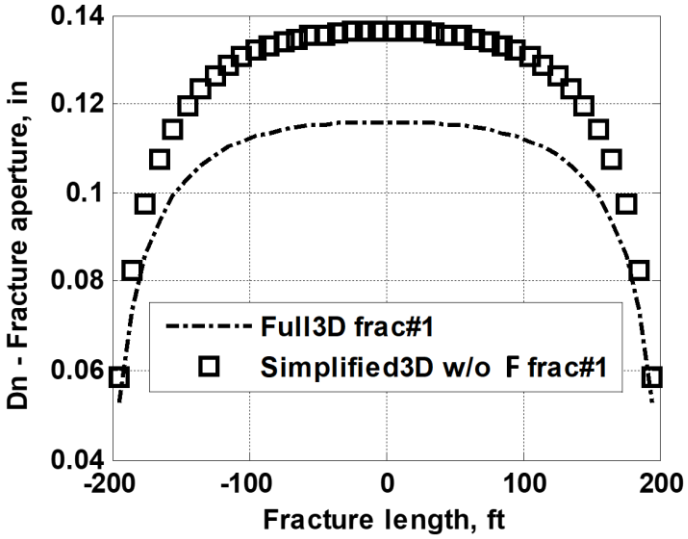

(a)

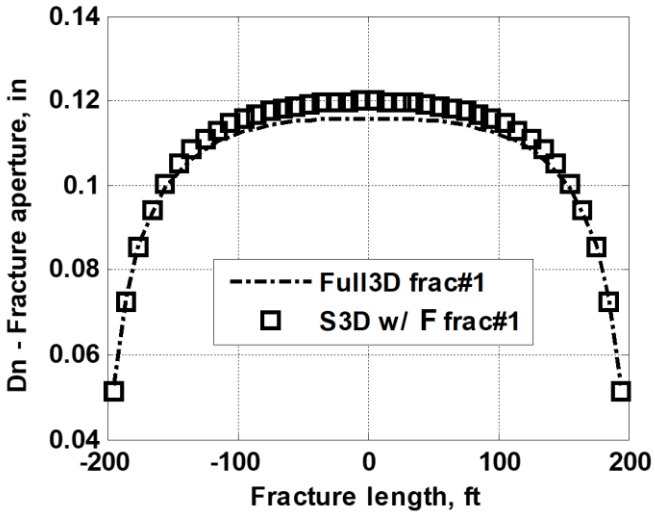

(b)

Figure 2.11: Fracture aperture versus length plots comparing fully 3D results and S3D results: (a) the original S3D DDM without stress correction; (b) the improved S3D DDM with stress correction.

2.5.4 Multiple Fractures in a Multi-layer Formation

In this section, a multi-fracture case is investigated to examine fracture interaction accuracy in multi-layer stress case. Figure 2.12 shows two fractures in a multi-layer formation and with perforations at different depths. The wellbores are overlapped from the top view and the two fractures are partially overlapped in the vertical and horizontal directions. The two fractures are assumed to have different heights, 100 ft for fracture #1 and 50 ft for fracture #2. Fracture #1 crosses all three layers, with most of the fracture height in layer #2. Fracture #2 is perforated in layer #1 and grows into the upper layer #2. In Table 2.4 a list of all input parameters is presented.

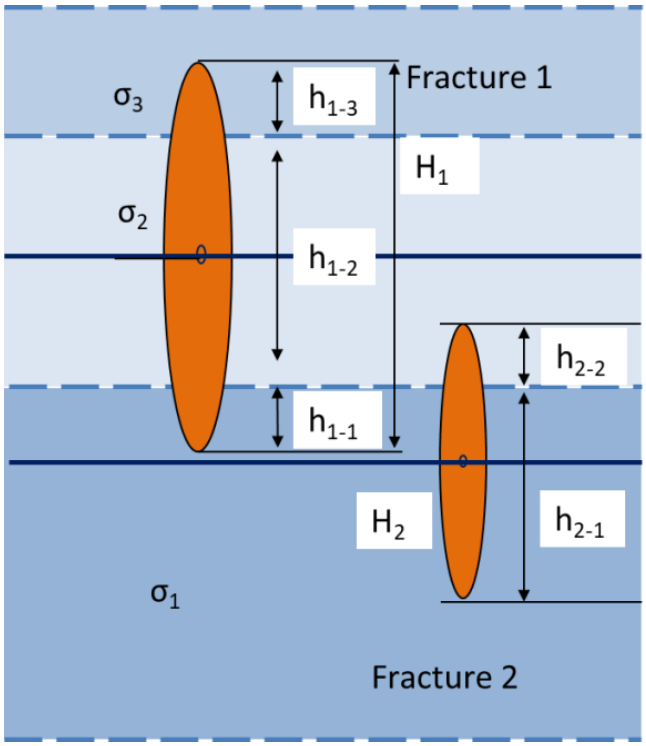

Figure 2.12: Side view of multiple fractures in a multi-layer formation.

Fracture length for fracture 1 (L_1)	800 ft
Fracture length for fracture 2 (L_2)	400 ft
Fracture height for fracture 1 (H_1)	100 ft
Fracture height for fracture 2 (H_2)	50 ft
Horizontal spacing	100 ft
Vertical spacing	50 ft
Minimum horizontal stress in layer 1 (σ_1)	6000 psi
Minimum horizontal stress in layer 2 (σ_2)	5700 psi
Minimum horizontal stress in layer 3 (σ_3)	5900 psi
Internal fluid pressure for fracture1 (P_{f1})	6200 psi
Internal fluid pressure for fracture1 (P_{f2})	6300 psi
Young's Modulus (E)	5×10^6 psi
Poison's ratio (v)	0.2
$h_{1\text{-}1}$, $h_{1\text{-}2}$, $h_{1\text{-}3}$	15, 70, 15 ft
$h_{2\text{-}1}$, $h_{2\text{-}2}$	40 ft, 10 ft

Table 2.4: Input parameters for multi-fracture in multi-layer case (in Figure 2.12).

The simulation results using the S3D method with and without the stress correction factor (F), are plotted respectively in Figure 2.12 and compared with fully 3D results. Similar to the previous sections, using the stress correction factor significantly improves the aperture result predictions to closely match the results of the fully 3D method (Figure 2.13). Also, fracture #2 has a much smaller aperture due to lower net pressure. Fracture #1 aperture is reduced in the part horizontally overlapped with fracture #2, which demonstrates the effect of stress shadowing. This last test case indicates that the improved S3D method fracture can accurately model multiple static fractures with non-uniform fracture height, vertical offset, and in-situ stress variation.

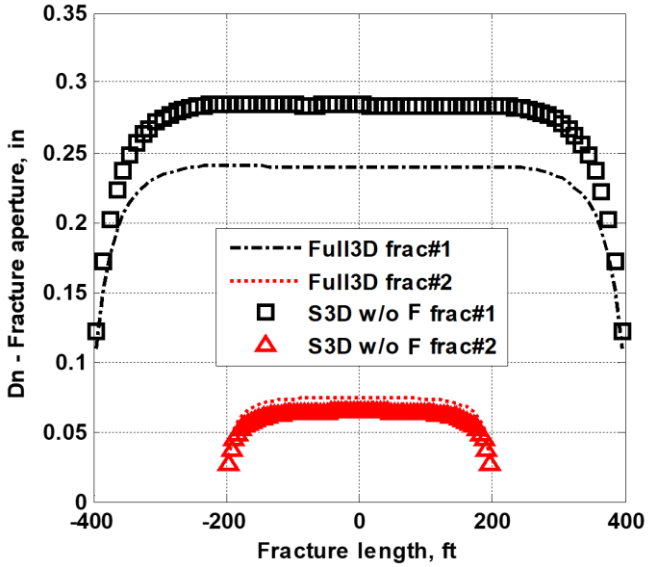

(a)

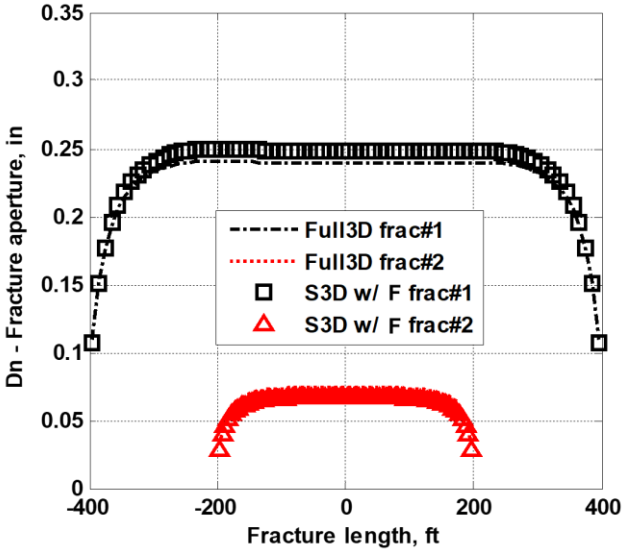

(b)

Figure 2.13: Fracture aperture versus length which compare the fully 3D results with S3D results: (a) the original S3D DDM without stress correction; (b) the improved S3D DDM with stress correction. In both figures, black lines are for fracture #1 and red lines for fracture #2.

2.6 CONCLUSIONS

This chapter proposes improvements to the simplified 3D displacement discontinuity method of Wu and Olson (2015) in order to analyze multiple fractures of non-uniform height in formations with layered stress. Two new correction factors are proposed and tested. The new 3D correction factor considers the effect of element aspect ratio and makes it possible to model fractures of non-uniform height. The stress correction factor gives the right effective net pressure for fracture aperture calculation by integrating the impact of varying in-situ stress at the fracture location.

Test cases demonstrate that the improved S3D method can accurately model multiple static fractures with non-uniform fracture height, vertical offset and in-situ stress variation. This improved model significantly extends the applicability of the S3D DDM approach for simulating realistic hydraulic fracturing problems while maintaining the considerably lower computation time and memory utilization of the original S3D approach.

Chapter 3: Simplified 3D Facture Propagation Model with a Novel Height Growth Function

In this chapter, an improved simplified 3D dynamic fracture model is developed to simulate single and multiple non-planar fracture propagation and height growth in layered formation. The model is then used to predict fracture height containment problems in a layered formation. The fracture propagation model can also be used to simulate multiple fracture propagation in a stacked pay development.

Following the numerical method introduced by Wu and Olson (2014), the model couples rock deformation and fluid mechanics. The improved S3D displacement discontinuity method presented in Chapter 2 is implemented in the model to calculate shear and normal displacement discontinuities, with stress shadowing effects taken into account. A novel fracture height growth methodology is developed to predict fracture height growth rate in layered stress conditions. The fracture width profile over the height is calculated by numerical solution calibrated analytical solution. Non-Newtonian fluid flow and the associated pressure drop in the fracture and well bore is iteratively coupled with the rock mechanics to simulate multi-frac propagation from a horizontal wellbore.

3.1 INTRODUCTION

There have been both numerical and experimental efforts to study fracture height growth mechanism and to explain related field observations (Warpinski, 1982; Jeffrey and Bunger, 2007; Gu and Siebrits, 2006; Dontsov and Peirce, 2015; Liu and Valko, 2017; Yue et al., 2018). Numerical modeling of fracture propagation in layered formation is increasingly important as stacked and staggered well placement has been tested and performed in the Horn River basin in Canada and the Permian and Delaware basins in the United States (Ueda et al, 2018), among other places. Among the concerning sub-processes in fracture propagation modeling, fracture height growth is one of the most important technical uncertainties in terms of well spacing design, reservoir drainage calculation and fracture interference prediction. Unexpected fracture penetration into the upper and lower layers could result in shorter fracture length propagation due to insufficient fracturing fluid. In the Midland basin, operators are trying to target up to four different formations from a single pad (Alimahomed et al., 2017). Figure 2.1 shows a "gun-barrel view" of an example well placement in the Spraberry, Wolfcamp and Cline formations, with a "wine-rack" pattern designed to co-develop Wolfcamp and Cline formations. In the stacked pay development, fracture height containment is crucial for well placement and determining the optimal rows of wells in the target formation interval.

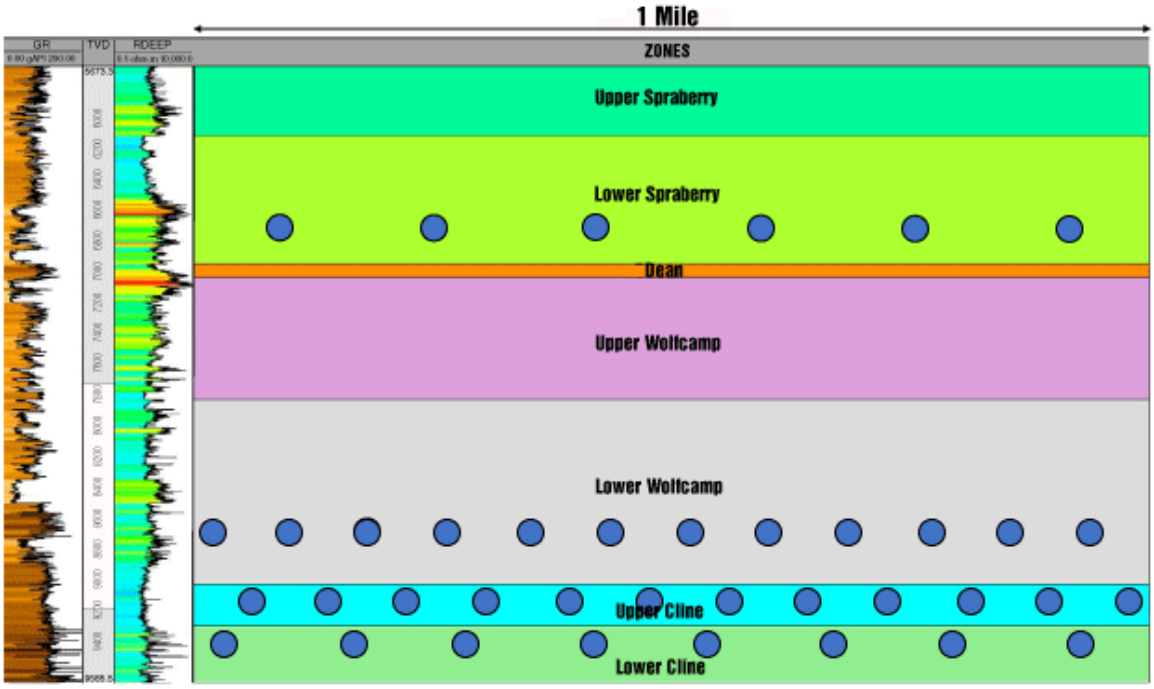

Figure 3.1: Gun barrel view of stacked and staggered wells in midland basin (from Alimahomed et al, 2018).

In this chapter, a novel height growth methodology is developed to predict fracture height profile in layered formation. The method, along with width profile calculation and the improved simplified 3D DDM introduced in Chapter 2, are implemented on the fracture propagation model developed by Wu and Olson (2014) to add a powerful height growth function. The new fracture propagation model is then validated against existing experimental and numerical results on fracture height growth.

3.2 Fracture Width Calculation in Vertical Direction

Understanding the variation of fracture width along fracture height is important for the material balance calculation in fracture propagation model. Fracture width at the upper and lower tips of the fracture is also a crucial input parameter for the height growth rate calculation presented later in Section 3.3.

The improved simplified 3D method proposed in Chapter 2 accurately predicted normal displacement discontinuity at the vertical center of fractures in a layered formation. Using only one row of fracture elements greatly reduces the computation time compared to standard fully 3D methods. However, the model has no degrees of freedom to calculate fracture width variation along the height. To solve for the vertical width profile for each element, an analytical solution is added to the model which is solved separately from the fundamental displacement discontinuity algorithm but dependent on the local DDM results.

The plane strain analytical solution for fracture opening in a layered formation, with in-situ stress variation and uniform mechanical properties, is given by Nolte and Economides (2000) as

$$\begin{aligned} w(z) &= \frac{4}{E'}[P_{cp} - \sigma_n]\sqrt{z(h-z)} \\ &+ \frac{4}{\pi E'}\sum_{i=1}^{n-1}(\sigma_{i+1} - \sigma_i)[(h_i - z)\cosh^{-1}\frac{z(\frac{h-2h_i}{h}) + h_i}{|z - h_i|}. \\ &+ \sqrt{z(h-z)\arccos(\frac{h-2h_i}{h})}] \end{aligned} \tag{3.1}$$

where E' is the plane strain modulus, h is the total height of the fracture, h_i is the height from fracture bottom tip to the top of layer i, P_{cp} and σ_n are the net pressure and normal stress at perforation position, σ_i is the normal stress acting on the fracture in layer i (Figure 3.2).

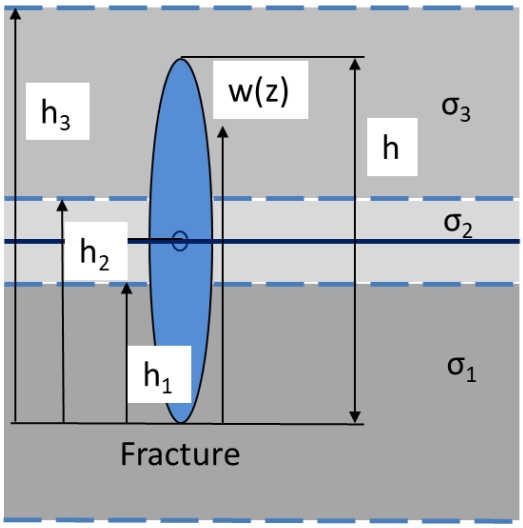

Figure 3.2: Illustration of the parameters in equation (3.1) (following Nolte and Economides, 2000).

The solution in equation (3.1) can be simplified as

$$w(z) = C_1\sqrt{z(h-z)} + C_2 f(z), \tag{3.2}$$

where

$$C_1 = \frac{4}{E'}[P_{cp} - \sigma_n]$$

$$C_2 = \frac{4}{\pi E'}$$

$$f(z) = \sum_{i=1}^{n-1}(\sigma_{i+1} - \sigma_i)[(h_i - z)\cosh^{-1}\frac{z(\frac{h-2h_i}{h}) + h_i}{|z - h_i|} + \sqrt{z(h-z)\arccos(\frac{h-2h_i}{h})}]$$

In this solution, the function *f(z)* calculates the effect of stress contrast between formation layers on the fracture opening at different vertical location *z*.

Fracture opening evaluated at the mid-point of fracture height ($z = h/2$) is derived as:

$$w(h/2) = C_1 \frac{h}{2} + C_2 f(\frac{h}{2}). \quad (3.3)$$

Fracture width or normal displacement discontinuity at the vertical center of each fracture element (D_n) is solved by S3D DDM introduced in chapter 2, which can be expressed as:

$$w(h/2) = D_n. \quad (3.4)$$

Combining equation (3.3) and equation (3.4) gives

$$C_1 \frac{h}{2} + C_2 f(\frac{h}{2}) = D_n. \quad (3.5)$$

The term A in equation (3.4) can be calculated by a simple equation manipulation:

$$C_1 = D_n - (\frac{h}{2} + C_2 f(\frac{h}{2})). \quad (3.6)$$

Plugging equation (3.6) back in equation (3.2) gives an equation where the analytical vertical width profile is dependent upon (or calibrated by) the DDM solution for each element along the length as

$$w(z) = (D_n - C_2 f(\frac{h}{2})) \frac{\sqrt{z(h-z)}}{h/2} + C_2 f(z), \quad (3.7)$$

where D_n is numerically derived fracture width at the vertical center, h is fracture height, and

$$C_2 = \frac{4}{\pi E'}$$

$$f(z) = \sum_{i=1}^{n-1} (\sigma_{i+1} - \sigma_i)[(h_i - z)\cosh^{-1}\frac{z(\frac{h-2h_i}{h}) + h_i}{|z - h_i|} + \sqrt{z(h-z)\arccos(\frac{h-2h_i}{h})}].$$

$$f(\frac{h}{2}) = \sum_{i=1}^{n-1} (\sigma_{i+1} - \sigma_i)[(h_i - \frac{h}{2})\cosh^{-1}\frac{(\frac{h-2h_i}{2}) + h_i}{|\frac{h}{2} - h_i|} + \sqrt{\frac{h^2}{4}\arccos(\frac{h-2h_i}{h})}]$$

3.3 A NOVEL METHOD TO CALCULATE FRACTURE HEIGHT GROWTH RATE

From the results of mechanical modeling, Olson (1993) proposed an expression for fracture propagation velocity as

$$V = A(\frac{K_{tip}}{K_{Ic}})^n, \tag{3.8}$$

where K_{tip} is the stress intensity factor at fracture tip, K_{Ic} is the critical fracture toughness, A is a constant of proportionality and n is the subcritical fracture growth index. The velocity index n is assumed to be 1 in this hydraulic fracturing study. Equation (3.8) can also be applied to the fracture top and bottom tips, giving the following location dependent equations,

$$V_L = A(\frac{K_{IL}}{K_{Ic}})^n, \tag{3.8a}$$

$$V_+ = A(\frac{K_{I+}}{K_{Ic}})^n, \tag{3.8b}$$

$$V_- = A(\frac{K_{I-}}{K_{Ic}})^n, \tag{3.8c}$$

where V_L, V_+ and V_- are the fracture propagation velocity at fracture lateral tip, top tip and bottom tip (Figure 3.3).

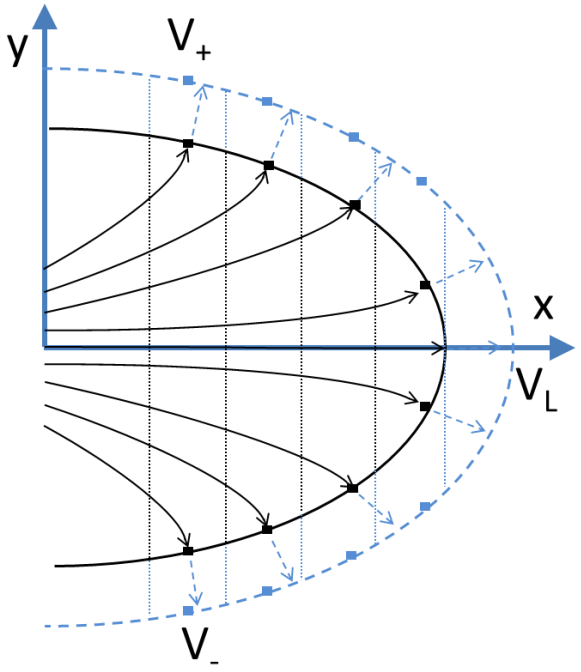

Figure 3.3: Illustration of hydraulic fracture propagation at fracture front (V_L), top (V_+) and bottom tip (V_-).

The fracture propagation rate at the fracture top or bottom tip can be expressed in terms of propagation velocity at the leading lateral edge ($y=0$) by combining equation (3.8a) and equation (3.8b) or equation (3.8c),

$$V_+ = A(\frac{K_{I+}}{K_{IL}})^n V_L\,, \tag{3.9a}$$

$$V_- = A(\frac{K_{I-}}{K_{IL}})^n V_L\,. \tag{3.9b}$$

In the fracture propagation model proposed by Wu and Olson (2014), V_L is constrained by fluid viscosity flow and therefore serves as a reference point for propagation velocity at top and bottom tips.

To obtain the fracture propagation velocities from equation (3.9), the stress intensity factor at the tip needs to be calculated. Olson (2007) gave the expression of Mode I stress intensity factor as a function of normal displacement discontinuity at the crack tip,

$$K_I = 0.806(\frac{\sqrt{\pi}E}{4(1-\nu^2\sqrt{\Delta a}})D_n\,, \tag{3.10}$$

where E is the Young's modulus, ν is the Poisson's ratio, Δa is the half element length, D_n is the normal displacement at fracture tip. Similarly, equation (3.9) is rewritten into three expressions by different fracture tip locations,

$$K_{IL} = 0.806(\frac{\sqrt{\pi}E}{4(1-\nu^2\sqrt{\Delta a}})D_{nL}\,, \tag{3.10a}$$

$$K_+ = 0.806(\frac{\sqrt{\pi}E}{4(1-\nu^2\sqrt{\Delta h}})D_{n+}\,, \tag{3.10b}$$

$$K_- = 0.806(\frac{\sqrt{\pi}E}{4(1-\nu^2\sqrt{\Delta h}})D_{n-} \tag{3.10c}$$

where K_{IL}, K_+ and K_- are the stress intensity factors at fracture lateral tip, top tip and bottom tip. The normal displacement discontinuity D_{nL} at the leading lateral tip can be computed from the improved S3D method discussed in Chapter 2. Fracture opening at the top and

bottom tips can be calculated from the fracture width profile function discussed in Section 3.2, and in this case, $D_{n+} = w(h)$ and $D_{n-} = w(0)$.

A common assumption for element-based fracture height calculation is to use the top or bottom fracture tip propagation velocity as the fracture height growth rate. Assuming the propagation velocity at each element is the vertical propagation rate rather than normal to the crack front tends to exaggerate growth rates near the wellbore, giving the characteristic "rat-tail" geometry. Figure 3.4 shows a common fracture shape from hydraulic fracture models assuming fracture top and bottom tips are only propagating in vertical direction. This geometry does not match experimental fracture propagation results and is thus considered to be relatively non-physical.

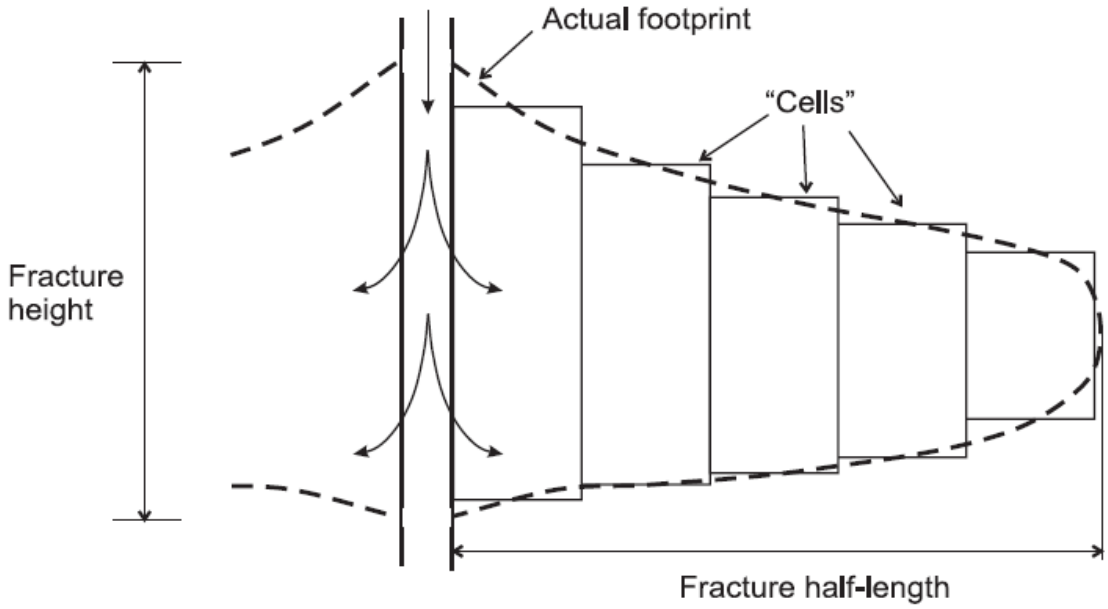

Figure 3.4: Illustration of simulated hydraulic fracture shape assuming fracture top and bottom tips are growing only in vertical directions (from Adachi et al., 2007).

In this study, the fracture propagation direction at the top and bottom tip of the fracture is assumed to be perpendicular to the fracture front. As shown in Figure 3.5, at step *n*, the top and bottom tip propagation velocity $\vec{u}$ is calculated by equation (3.9), with a direction perpendicular to the fracture front of previous step *n-1*, which is the black solid line. The fracture front location of step *n* is interpolated using the tip velocity $\vec{u}_i$ at each fracture element, shown by the blue dash line. Fracture height growth rate for step *n* is the vertical distance (*Δh*) between fracture front at step *n* and step *n-1* at each element location, divided by the time step.

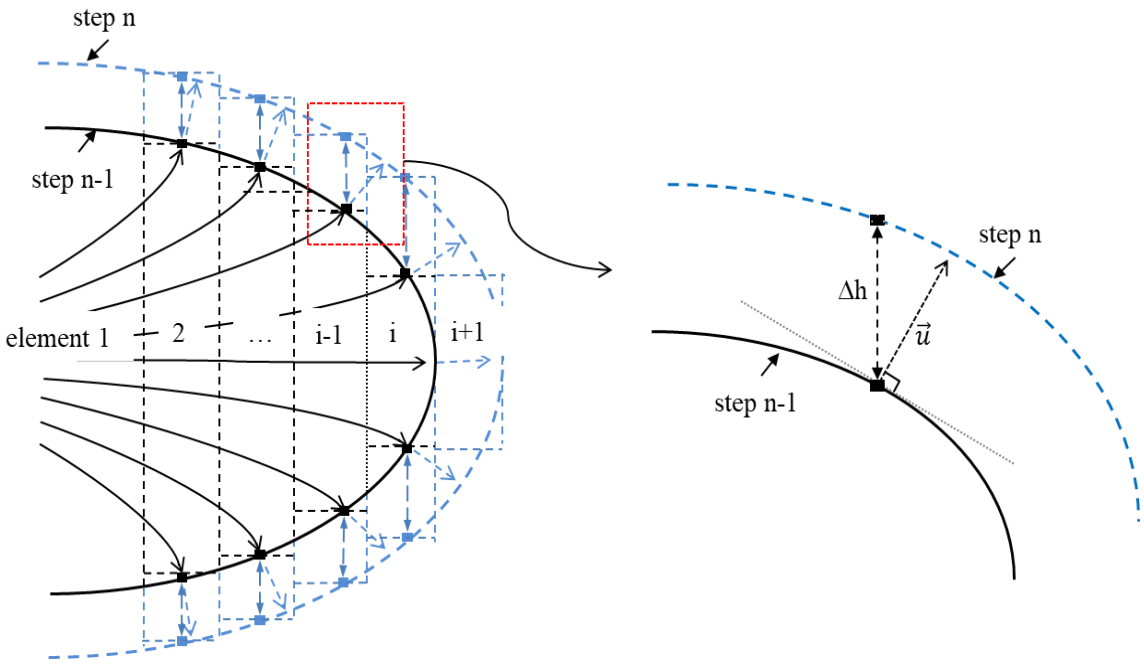

Figure 3.5: Illustration of fracture propagation from step *n-1* (black solid line) to step *n* (blue dash line), assuming fracture propagation direction on top and bottom tip is perpendicular to fracture front.

3.4 NUMERICAL IMPLEMENTATION

We have implemented 1) the improved S3D DDM from Chapter 2, 2) the width profile function from Section 3.2 and 3) the height growth algorithm introduced in Section 3.3 to the fracture propagation model.

Wu and Olson (2014) proposed a multiple fracture propagation model by iteratively coupling rock mechanics and fluid mechanics (Figure 3.6). The model assumed homogenous medium and constant fracture height which is applicable to well-contained hydraulic fractures in the unconventional reservoirs.

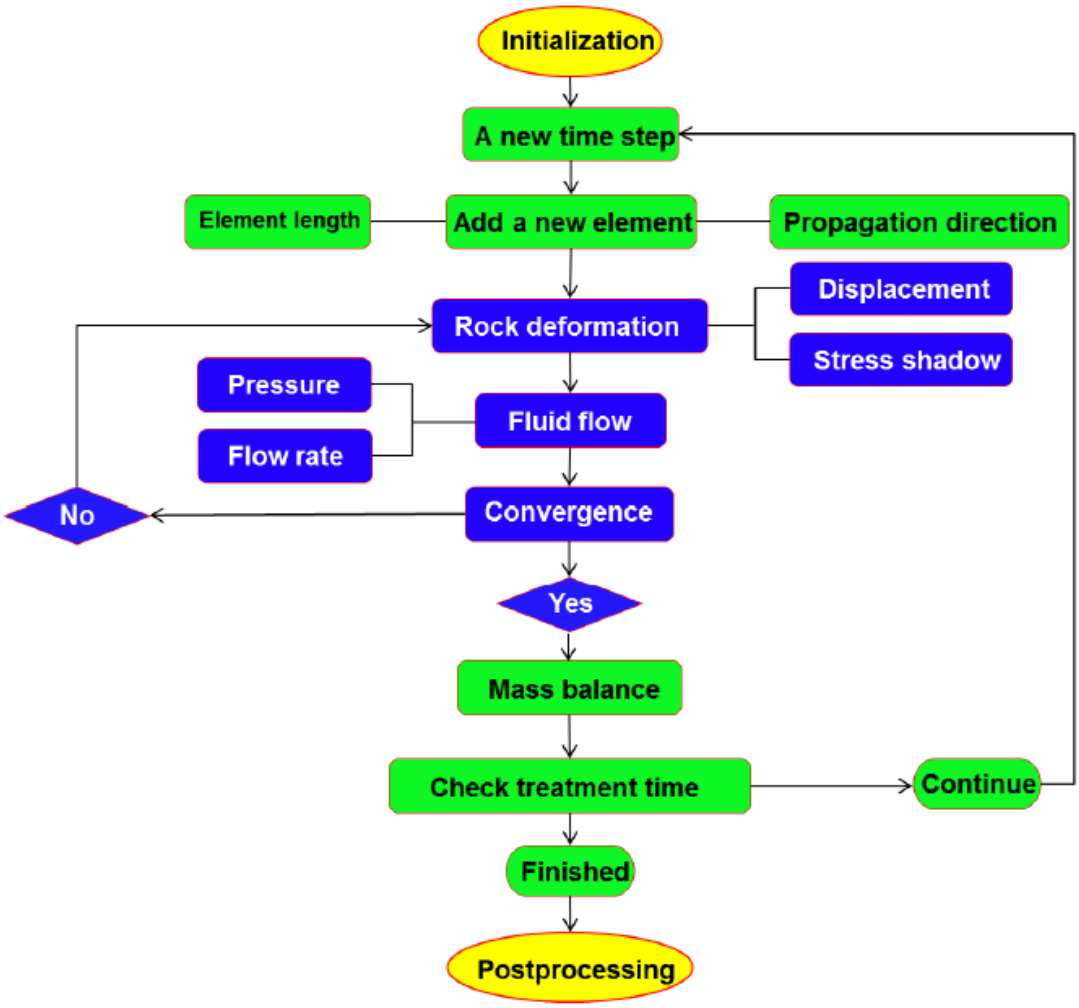

Figure 3.6: Flow chart of time-step loop of the iteratively coupled solution (from Wu and Olson, 2014).

The improved S3D DDM presented in Chapter 2 extends the rock mechanics solution to fractures with non-uniform height in formation with multiple stress layers. In Section 2.2 and 2.3, the width profile function and the fracture height growth methodology are introduced to allow dynamic fracture growth in the propagation model. The above functions are implemented to the coupled solution from Wu and Olson (2014). A novel

multi-fracture propagation model with height growth is shown by the new flow chart in Figure 3.7.

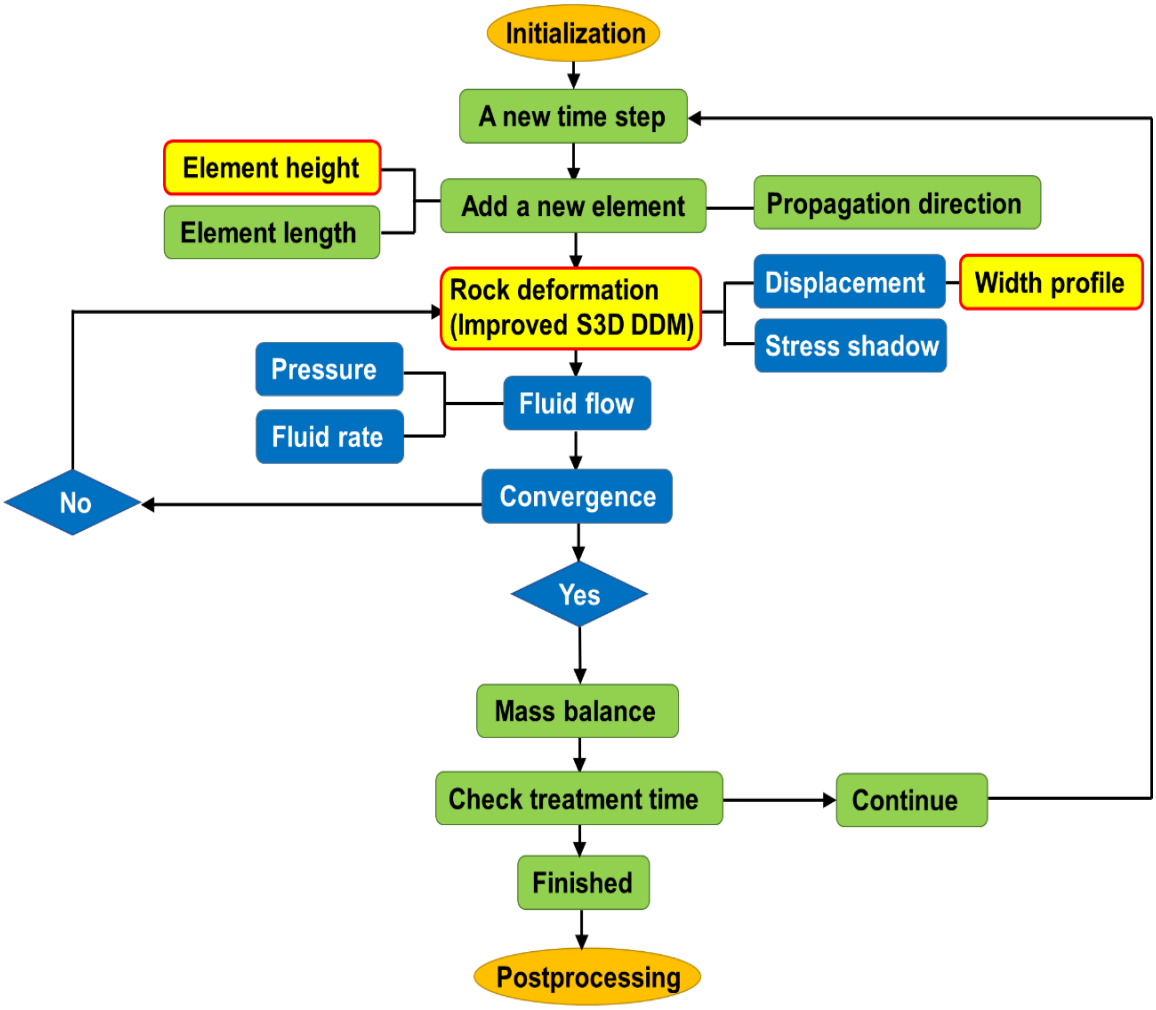

Figure 3.7: Flow chart of a novel multi-fracture propagation model with height growth.

3.5 MODEL VALIDATION

3.5.1 Validation of the Width Profile Function

The accuracy of the semi-analytical fracture width solution is investigated by simulating a single uniformly pressured fracture in a multi-layer formation with different in-situ stresses in the layers. Table 3.1 presents the parameters assumed in the model. Figure 3.8 shows the in-situ stress distribution in vertical layers.

Fracture half length (L_h)	400 ft
Fracture height (H)	100 ft
Young's Modulus (E)	5×10^6 psi
Poison's ratio (v)	0.2
Fracture internal fluid pressure (P_f)	6100 psi

Table 3.1: Input parameters for modeling fracture width profile in a layered reservoir.

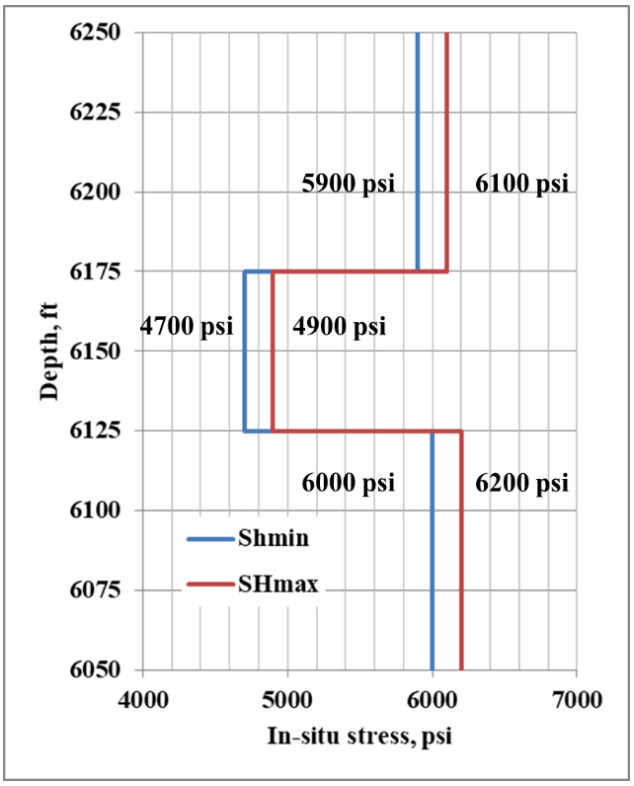

Figure 3.8: The assumed in-situ stress variation in the multi-layer reservoir for fracture width model comparison.

For the semi-analytical solution, the fracture width at the center of the fracture height is first calculated using S3D DDM. Then the vertical profile of the fracture width is generated with the semi-analytical solution. The results are compared to the fully 3D method using 21 rows of elements in vertical direction.

Figure 3.9 depicts the fracture width profile for each element using the semi-analytical solution and the fully 3D method. For both methods, the fracture width profile is evaluated at 40 horizontal locations throughout fracture half length. Each curve in the figure represents the fracture width profile evaluated cross a vertical section of the fracture. Fracture opening has the largest value near the wellbore and deceases moving towards the fracture tip. The arrow is pointing from near wellbore sections to fracture tip sections in

horizontal direction. The variation of in-situ stresses is reflected by both method. There is a reduction in fracture width when the fracture crosses out of the middle low-stress layer and into the outer high-stress layers on the top and bottom.

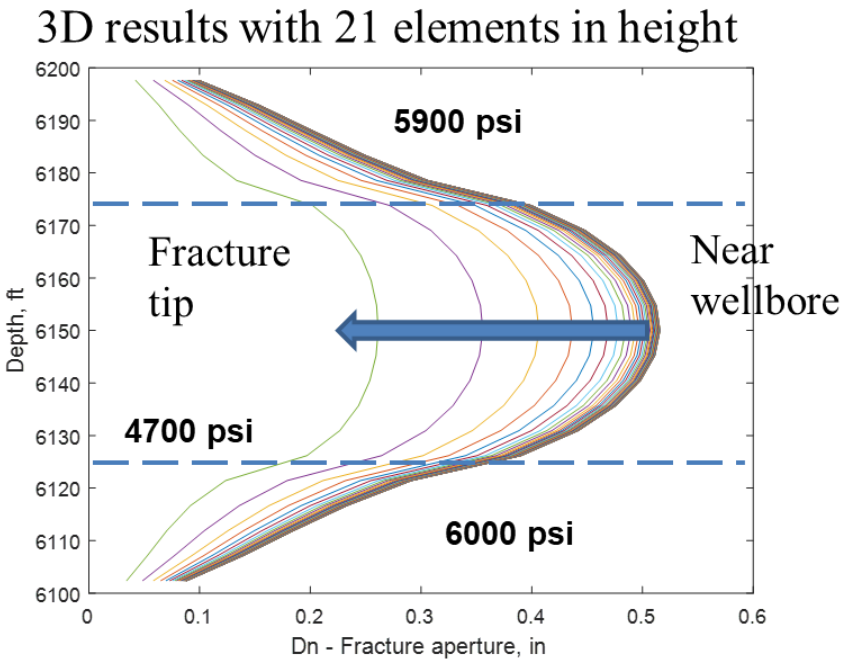

(a)

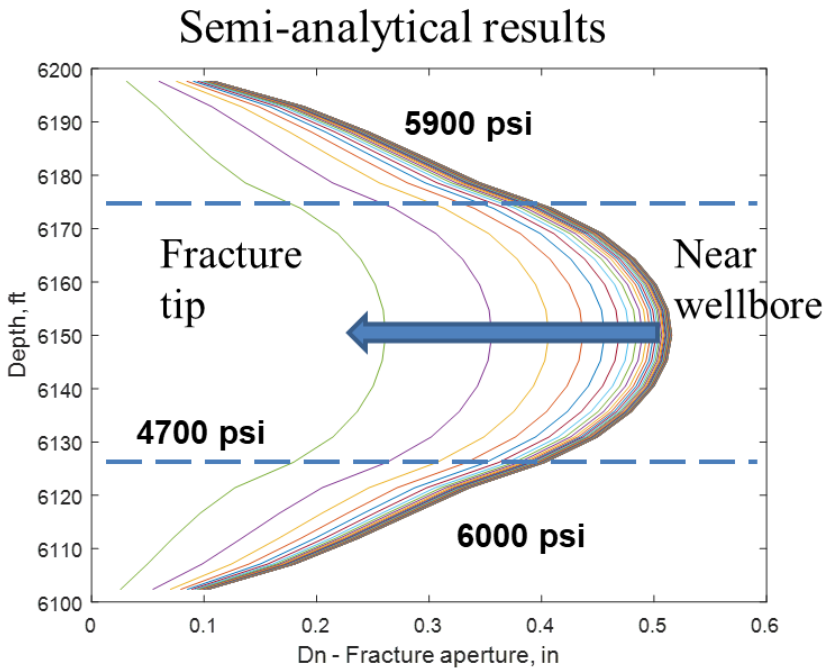

(b)

Figure 3.9: (a) Fracture width profiles simulated by fully 3D DDM; (b) Fracture width profiles simulated by the semi-analytical solution.

The difference is really small as we compare the fracture width profiles generated using both methods (Figure 3.10). The relative error for all curves combined is less than 10%, when comparing the semi-analytical solution with fully 3D method with 21 elements in height. The relative error is 14% between the semi-analytical solution and the fully 3D method with half amount of the elements (11 elements) in height. The error between two method decreases as the number of vertical element in the fully 3D method increases. Since the fully 3D method is more reliable with more elements, the semi-analytical solution is demonstrated to be accurate.

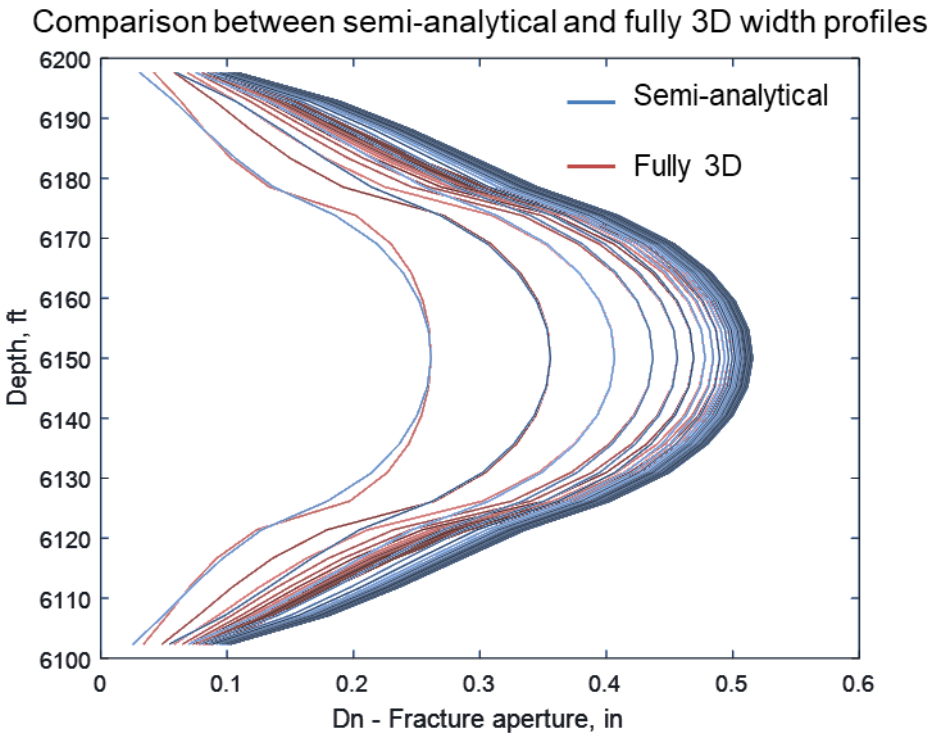

Figure 3.10: Comparison of fracture width profile generated using semi-analytical method (blue) and fully 3D (red) method with 21 elements in vertical direction.

3.5.2 Validation of the Improved Fracture Propagation Model

For validation, we run the simulator to reproduce a well-documented experiment. Jeffrey and Bunger (2007) performed a laboratory hydraulic fracturing experiment by injecting dyed viscous fluid into man-made polymethyl methacrylate (PMMA) blocks with step-like stress changes on the interface. The experiment down-scaled and mimicked the layered formation condition commonly found in unconventional shale reservoirs. In the experiment, the fracture geometry and opening were measured by analyzing the light intensity in images of the growing fracture, and the injection rate and pressure data were also recorded. Table 3.2 summarized the parameters used in the experiment.

	SI	Oil field
Injection rate, Q	$1.70\times10^{-9}\ m^3/s$	6.4×10^{-7} bbl/min
Fluid viscosity, μ	30.2 Pa·s	30200 cp
Young's modulus, E	3300 Mpa	4.8×10^{5} psi
Poisson's ratio, ν	0.4	0.4
Stress in perf layer, σ_p	2.2 MPa	319 psi
Stress in barrier layer, σ_b	6.5 MPa	943 psi
Stress contrast, $\Delta\sigma$	4.3 MPa	624 psi
Perf layer height, H	0.05 m	0.164 ft

Table 3.2: Parameters in both oil field and SI units for the fracturing experiment conducted by Jeffery and Bunger (2007), and the same inputs are used in validating the fracture propagation model.

The researchers created high stress layers on the top and bottom of the perforated layer and the stress contrast was 624 psi or 4.3 MPa. A constant injection rate was maintained at 6.4×10^{-7} bbl/min. The total injection time for the experiment was 600s and then the system was shut in after the injection. Figure 3.11 shows the fracture shape observed at four different times during the experiment (Jeffery and Bunger, 2007).

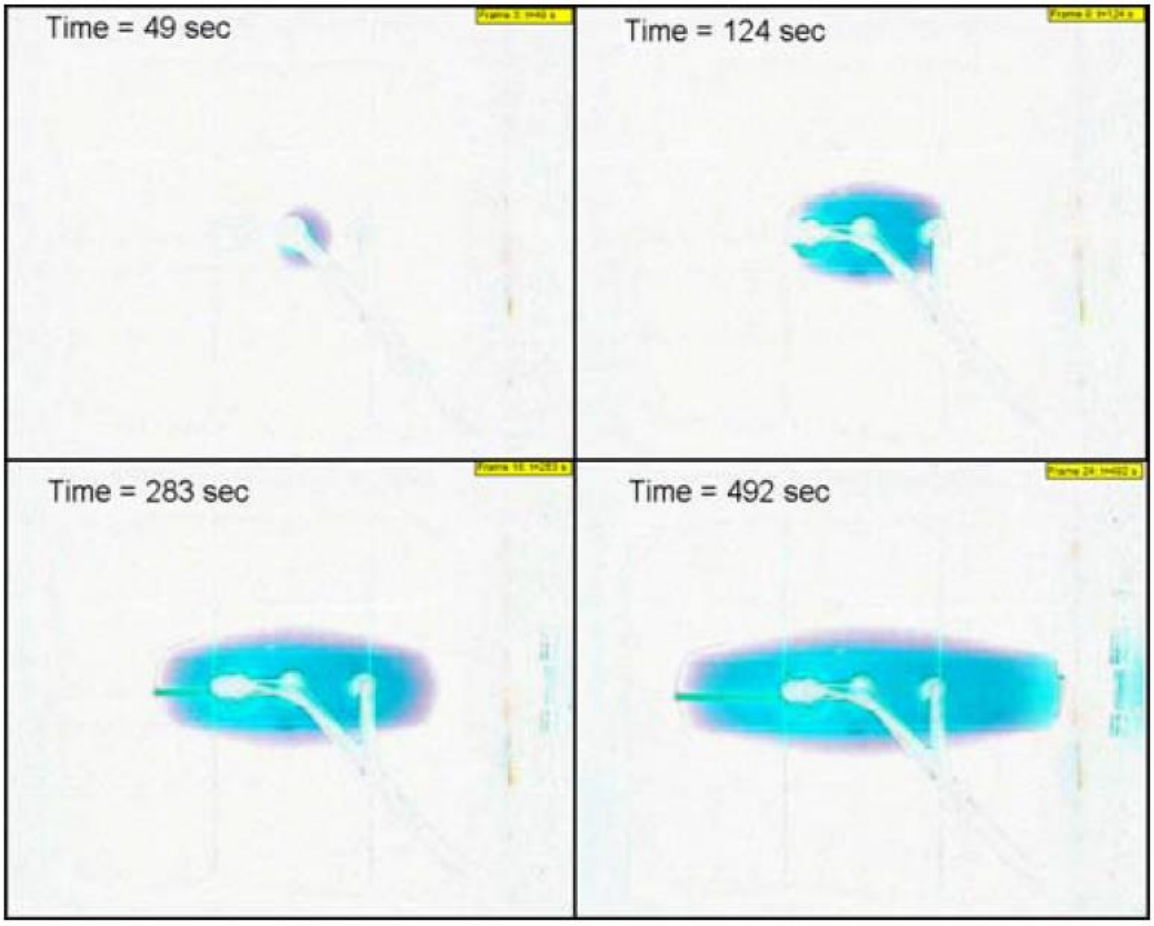

Figure 3.11: The fracture shape observed at four different time during the fracturing experiment (from Jeffery and Bunger, 2017).

Figure 3.12 shows maps of the simulated fracture geometry for similar time as the four experiment photos in Figure 3.11. Similar fracture geometries are recorded by both experiment and model simulation at different stages of injection. In early stage, top and bottom tips of the fracture haven't penetrated into the high-stress barrier layers and the fracture has a penny-shape. Later when the fracture height reached and exceeded the thickness of perf layer, the fracture height growth rate sharply decreased. Since the fracture height growth is relatively limited, the fracture propagates more laterally than vertically.

The fracture model also captured the width variation along fracture height direction. Fracture opening in the barrier layer is reduced due to higher in-situ stresses.

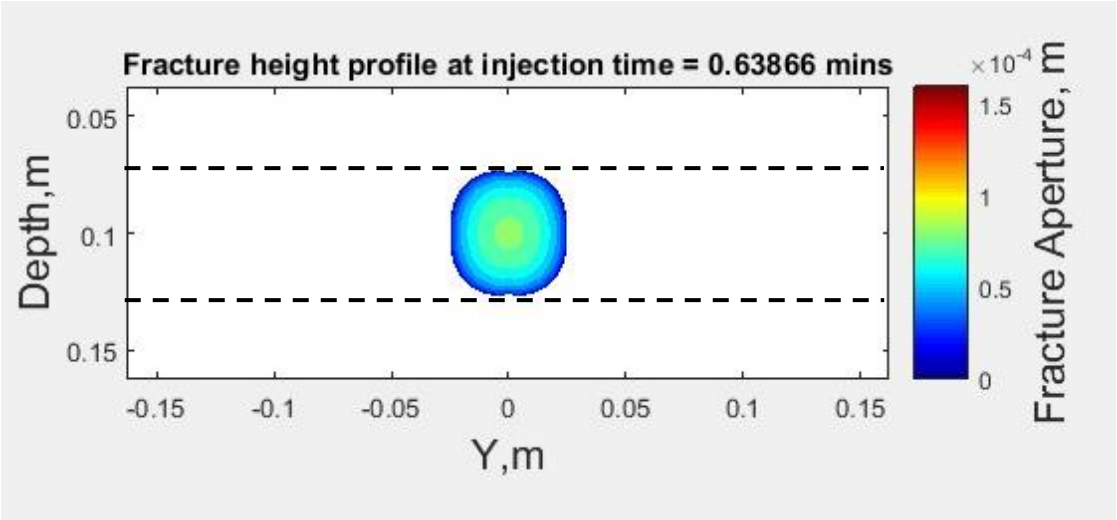

(a)

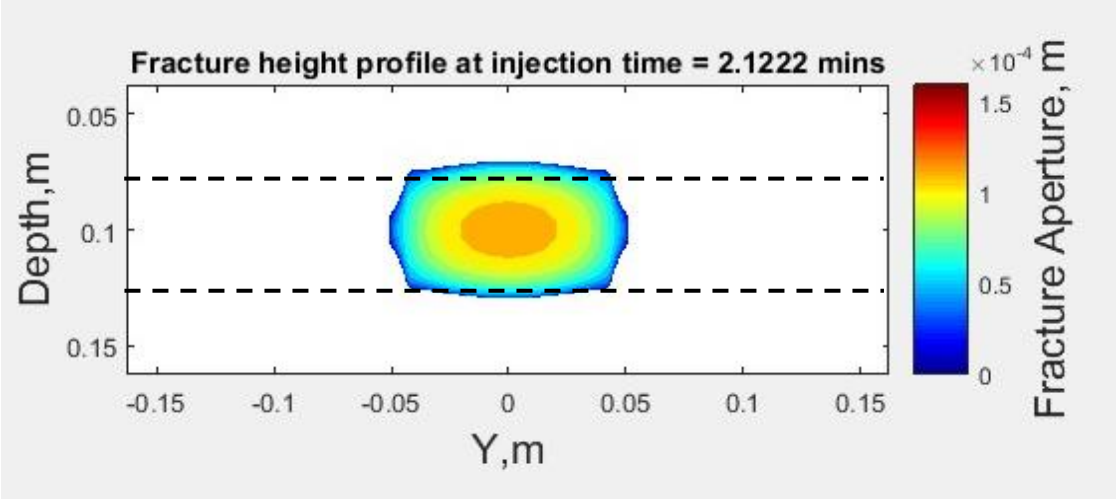

(b)

Figure 3.12: (continued on next page).

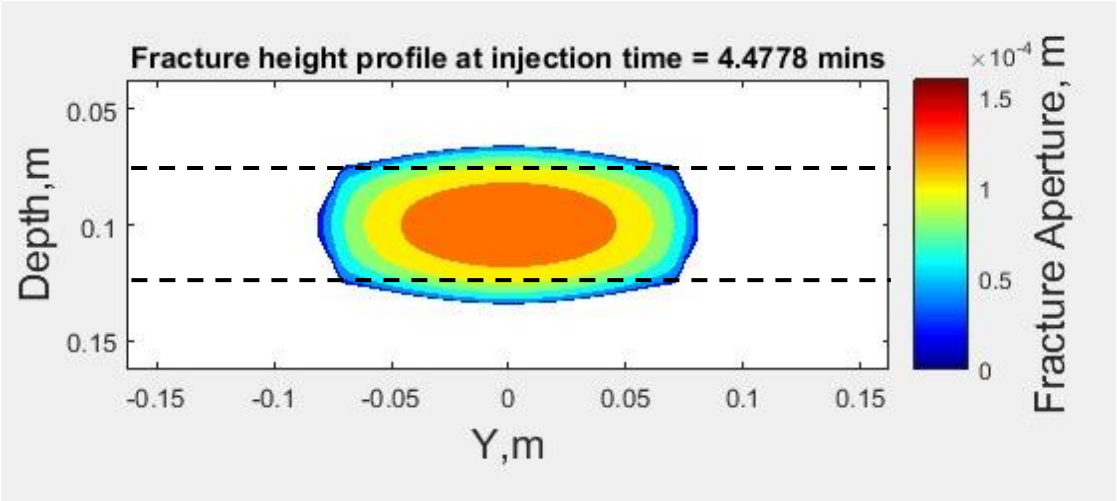

(c)

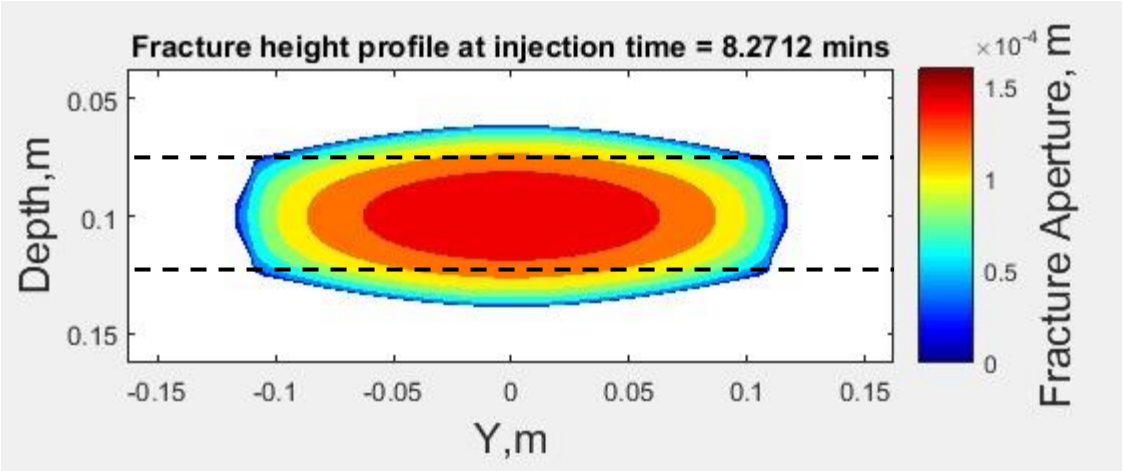

(d)

Figure 3.12: Gun-barrel view of fracture shape at four different times during the simulation. *y* is the fracture length direction and depth is the fracture height direction. The color inside the fracture represents fracture opening. The dashed lines highlighted the stress-contrast interfaces between per layer and barrier layers.

Other researchers have also tried to simulate the mentioned experimental results using numerical methods. Figure 3.13 shows the comparison of experimental fracture geometry at late time (Jeffery and Bunger, 2007) with 1) the new fracture propagation model of this thesis, 2) a conventional P3D model, 3) the fully-planar Implicit Level Set Algorithm (ILSA) scheme (Dontsov and Peirce, 2015; Peirce and Detournay, 2008). The conventional P3D method overestimated the fracture height. The new fracture propagation model predicts a similar fracture geometry as ILSA, matching the wellbore height and overall length seen in the experiment. Meanwhile, the computation time of the proposed model is smaller by at least two orders of magnitude than full 3D simulators and ILSA.

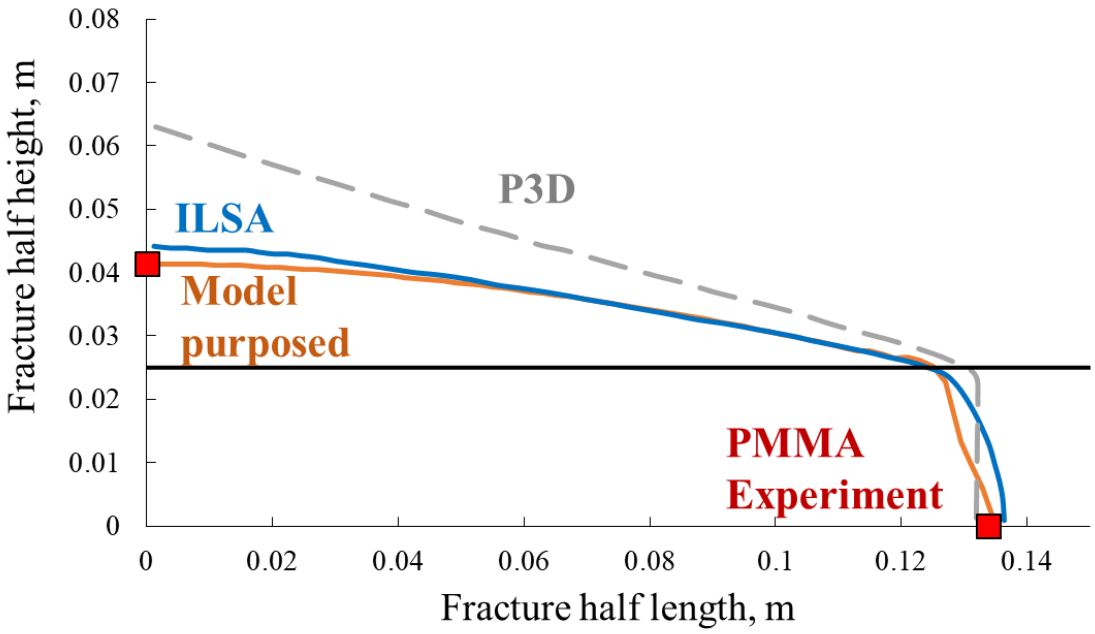

Figure 3.13: Comparison of the simulation results from the new fracture propagation model (orange solid line), conventional pseudo-3D method (grey dashed line), ILSA (blue solid line) and experimental result (red squares).

3.6 CONCLUSIONS

In this Chapter, the original fracture propagation model from Wu and Olson (2015) is further improved to predict fracture width profile in vertical direction and fracture height growth rate in layered formations. The proposed semi-analytical fracture width function utilized results from numerical method to calibrate the analytical solution predictions. A novel fracture height growth methodology is introduced to predict fracture height in layered formations. The geometric transformation from tip propagation velocity to fracture height growth rate enables the model to avoid common pitfalls of over-predicting the fracture height.

The accuracy of the improved fracture propagation model is examined by a case study using experimental inputs. The proposed model successfully simulated the experimental result and some numerical results from other researchers. The improved S3D fracture propagation model provides an efficient and reliable method for simulating multiple fracture propagation in multi-layer systems. The relationships derived for fracture width profile and fracture height growth should also be adaptable to other 3D fracture models for improved accuracy and better computational efficiency.

Chapter 4: Conclusions and Future Work

4.1 Summary of Completed Work

In this master's thesis, an improved simplified 3D (S3D) hydraulic fracture model is developed. The improved model is capable of simulating single and multiple non-planar fracture propagation and height growth in layered reservoir formations with different in-situ stresses. The following is a list of new methods employed in the static model and the dynamic model.

For the static fracture model:

- A new 3D correction factor is applied in the S3D DDM which considers the effect of element aspect ratio and makes it possible to model fractures of non-uniform height.
- A stress correction factor is employed to calculate the influence of stress contrast between layers on fracture opening. Static simulation results from the improved model compare favorably with reference analytical solutions for penny-shaped fractures and with fully 3D numerical solutions.
- Test cases demonstrate that the improved S3D method can accurately model multiple static fractures with non-uniform fracture height, vertical offset and in-situ stress variation while maintaining the considerably lower computation time.

For the dynamic fracture model:

- The fracture width profile along the vertical direction in a layered reservoir is calculated by an analytical solution dependent on the local DDM results.
- A novel fracture height growth methodology is introduced to predict fracture height in layered formations. The geometric transformation from

tip propagation velocity to fracture height growth rate enables the model to avoid common pitfalls of over-predicting the fracture height.

4.1 FUTURE WORK

Research work presented in the thesis could be extended by topics including but not limited to (1) fracture propagation in layered reservoirs with different mechanical properties, (2) non-planar fracture height development, and (3) 3D interaction between natural and hydraulic fractures.

In this study, we studied the rock mechanics for fractures in layered reservoir with different in-situ stresses. Another uncertainty in layered reservoirs is changing of mechanical properties. Variation of mechanical properties such as Young's modulus and Poisson's ratio between layers affects fracture height growth in indirect ways. Yue et al. (2018) studied the impact of modulus values, fracture tip location and height percentage of rock layers on calculating effective modulus of a layered reservoir. This novel effective modulus approach can be applied into the current improved S3D multi-fracture model to simulate fracture propagation in layered formation with both in-situ stress and mechanical property variations.

The multi-fracture propagation model can be extended to simulate fracture turning in vertical direction. The current model is capable of solving non-planar fracture propagation in horizontal direction. Field observations suggest fracture growth in vertical direction could be non-planar and complicated. To better simulate fracturing treatment in field operations, nonplanar fracture propagation in vertical direction could be studied. One of the possible approaches is to add rows of element in the vertical direction and calculate the 3D stress field around the fractures.

The interaction of natural and hydraulic fractures was studied by Wu and Olson (2015) considering fracture coalescence and fluid flow into the natural fractures. In this study, we added the fracture height growth function and the fracture is no longer contained by the target layer. To model the interaction between natural fractures and hydraulic fractures with non-uniform height, fluid flow equation needs to be modified to count the change of flowing area. In addition, the interaction criterion and activation of natural fractures may be affected by the fracture height variation. Future work may involve both numerical and experimental efforts to study the complex hydraulic and natural fracture interactions.

Glossary

σ_{ii}	Stress components, i = 1,2,3
x_i	Distance in local coordinates, i = 1,2,3
a & b	Half-length and height in local coordinates
D_1 *or* D_n	Normal displacement discontinuities or fracture aperture
D_3 *or* D_s	Shear displacement discontinuities
ν	Poisson's ratio
L_e	Element length
H_e	Element height
C_{11}& C_{13}	3D correction factors
d	Distance between elements
H *or* h	Fracture height
P *or* P_{cp}	Effective pressure
P_f	Fluid pressure inside fracture
σ_n	Normal stress in perforation layer
F	Stress correction factor
E'	Plane strain modulus
σ_i	Normal stress in layer i
h_i	Height interval in layer i
z_i	Height at the center of fracture segment in layer i
G	Shear modulus
E	Young's Modulus
w	Fracture opening
K_{tip}	Stress intensity factor at fracture tip
K_{Ic}	Critical fracture toughness
n	Subcritical fracture growth index

A	Constant of proportionality in the fracture propagation velocity equation
K_{IL}, K_{I+}, K_{I-}	Stress intensity factor at fracture front, top and bottom tip
V_L, V_+ , V_-	Fracture propagation velocity at fracture front, top and bottom tip
Δa	Half element length
D_L, D_{n+}, D_{n-}	Fracture opening at fracture front, top and bottom tip
Q	Injection rate
μ	Fluid viscosity

References

Adachi, J., Siebrits, E., Peirce, A. and Desroches, J., 2007. Computer simulation of hydraulic fractures. International Journal of Rock Mechanics and Mining Sciences, 44(5), pp.739-757.

Alimahomed, F., Malpani, R., Jose, R., Haddad, E., Arteaga, E.V., Smith, L. and Lati, S., 2017, September. Stacked Pay Pad Development in the Midland Basin. In SPE Liquids-Rich Basins Conference-North America. Society of Petroleum Engineers.

Blanton, T.L. and Olson, J.E., 1997, January. Stress magnitudes from logs: effects of tectonic strains and temperature. In SPE Annual Technical Conference and Exhibition. Society of Petroleum Engineers.

Cheng, Y., 2009, January. Boundary element analysis of the stress distribution around multiple fractures: implications for the spacing of perforation clusters of hydraulically fractured horizontal wells. In SPE Eastern Regional Meeting. Society of Petroleum Engineers.

Crouch, S.L. and A.M. Starfield. 1983. Boundary element methods in solid mechanics. 1st ed. London: George Allen & Unwin.

Dontsov, E.V. and Peirce, A.P., 2015. An enhanced pseudo-3D model for hydraulic fracturing accounting for viscous height growth, non-local elasticity, and lateral toughness. Engineering Fracture Mechanics, 142, pp.116-139.

Economides, M. and Nolte, K.G., 2000. In Reservoir Stimulation, 3rd, Chichester, NY: John Wiley & Sons, 6-16.

Economides, M.J., Hill, A.D., Ehlig-Economides, C. and Zhu, D., 2012. Petroleum Production Systems: Pearson Education. Original edition. ISBN, 496500264.

Elbel, J.L., Piggott, A.R. and Mack, M.G., 1992, January. Numerical modeling of multilayer fracture treatments. In Permian Basin Oil and Gas Recovery Conference. Society of Petroleum Engineers.

Ferrill, D.A., McGinnis, R.N., Morris, A.P., Smart, K.J., Sickmann, Z.T., Bentz, M., Lehrmann, D. and Evans, M.A., 2014. Control of mechanical stratigraphy on bed-restricted jointing and normal faulting: Eagle Ford Formation, south-central Texas. AAPG Bulletin, 98(11), pp.2477-2506.

Fisher, M.K., Heinze, J.R., Harris, C.D., Davidson, B.M., Wright, C.A. and Dunn, K.P., 2004, January. Optimizing horizontal completion techniques in the Barnett shale using microseismic fracture mapping. In SPE Annual Technical Conference and Exhibition. Society of Petroleum Engineers.

Fisher, M. K., and Warpinski, N. R. 2012. Hydraulic-fracture-height growth: real data. SPE Production & Operations, 27(01), pp. 8-19.

Fung, R.L., Vilayakumar, S. and Cormack, D.E., 1987. Calculation of vertical fracture containment in layered formations. SPE formation evaluation, 2(04), pp.518-522.

Geertsma, J. and De Klerk, F., 1969. A rapid method of predicting width and extent of hydraulically induced fractures. Journal of Petroleum Technology, 21(12), pp.1-571.

Green, A.E. and Sneddon, I.N., 1950, January. The distribution of stress in the neighbourhood of a flat elliptical crack in an elastic solid. In Mathematical Proceedings of the Cambridge Philosophical Society (Vol. 46, No. 1, pp. 159-163). Cambridge University Press.

Gu, H. and Siebrits, E., 2006, January. Effect of formation modulus contrast on hydraulic fracture height containment. In International Oil & Gas Conference and Exhibition in China. Society of Petroleum Engineers.

Jeffrey, R.G. and Bunger, A., 2009. A detailed comparison of experimental and numerical data on hydraulic fracture height growth through stress contrasts. SPE Journal, 14(03), pp.413-422.

Khristianovich, S. A., and Yu P. Zheltov. "Hydraulic Fracture of on Oil-Bearing Reservoir." Izv. Akad. Nauk SSSR, ONT 5 (1955): 3-41.

Liu, S. and Valkó, P.P., 2015, February. An improved equilibrium-height model for predicting hydraulic fracture height migration in multi-layered formations. In SPE Hydraulic Fracturing Technology Conference. Society of Petroleum Engineers.

Mack, M.G., Elbel, J.L. and Piggott, A.R., 1992, January. Numerical representation of multilayer hydraulic fracturing. In The 33th US Symposium on Rock Mechanics (USRMS). American Rock Mechanics Association.

Mayerhofer, M. J., Stegent, N. A., Barth, J. O., and Ryan, K. M. 2011. Integrating fracture diagnostics and engineering data in the Marcellus shale. In proceedings of the SPE Annual Technical Conference and Exhibition, Denver, Colorado, USA.

McClure, M.W., 2012. Modeling and characterization of hydraulic stimulation and induced seismicity in geothermal and shale gas reservoirs (Doctoral dissertation, Stanford University).

McClure, M.W. and Kang, C.A., 2017, February. A Three-Dimensional Reservoir, Wellbore, and Hydraulic Fracturing Simulator that is Compositional and Thermal, Tracks Proppant and Water Solute Transport, Includes Non-Darcy and Non-Newtonian Flow, and Handles Fracture Closure. In SPE Reservoir Simulation Conference. Society of Petroleum Engineers.

Miskimins, J.L. and Barree, R.D., 2003, January. Modeling of hydraulic fracture height containment in laminated sand and shale sequences. In SPE Production and Operations Symposium. Society of Petroleum Engineers.

Nordgren, R.P., 1972. Propagation of a vertical hydraulic fracture. Society of Petroleum Engineers Journal, 12(04), pp.306-314.

Nichols, G., 2009. Sedimentology and stratigraphy. John Wiley & Sons.

Olson, J.E., 1993. Joint pattern development: Effects of subcritical crack growth and mechanical crack interaction. Journal of Geophysical Research: Solid Earth, 98(B7), pp.12251-12265.

Olson, J.E., Laubach, S.E. and Lander, R.H., 2009. Natural fracture characterization in tight gas sandstones: Integrating mechanics and diagenesis. AAPG bulletin, 93(11), pp.1535-1549.

Olson, J.E., 2007. Fracture aperture, length and pattern geometry development under biaxial loading: a numerical study with applications to natural, cross-jointed systems. Geological Society, London, Special Publications, 289(1), pp.123-142.

Olson, J.E. and Wu, K., 2012, January. Sequential vs. simultaneous multizone fracturing in horizontal wells: insights from a non-planar, multifrac numerical model. In SPE Hydraulic Fracturing Technology Conference. Society of Petroleum Engineers.

Peirce, A. and Detournay, E., 2008. An implicit level set method for modeling hydraulically driven fractures. Computer Methods in Applied Mechanics and Engineering, 197(33-40), pp.2858-2885.

Perkins, T.K. and Kern, L.R., 1961. Widths of hydraulic fractures. Journal of Petroleum Technology, 13(09), pp.937-949.

Pollard, D.D. and Segall, P., 1987. In Fracture mechanics of rock.

Rongved, L. and Hill, N.J., 1957. Dislocation over a bounded plane area in an infinite solid. J. Appl. Mech, 24, pp.252-254.

Roussel, N.P. and Sharma, M.M., 2011. Optimizing Fracture Spacing and Sequencing in Horizontal-Well Fracturing. SPE Prod & Oper 26 (2): 173–184. SPE-127986-PA. http://dx. doi. org/10.2118/127986-PA.

Salamon, M.D.G., 1964. Elastic analysis of displacements and stresses induced by the mining of seam or reef deposits: Part II: Practical methods of determining displacement, strain and stress components from a given mining geometry. Journal of the Southern African Institute of Mining and Metallurgy, 64(6), pp.197-218.

Savitski, A.A. and Detournay, E., 2002. Propagation of a penny-shaped fluid-driven fracture in an impermeable rock: asymptotic solutions. International Journal of Solids and Structures, 39(26), pp.6311-6337.

Segedin, C.M., 1951, April. Note on a penny-shaped crack under shear. In Mathematical Proceedings of the Cambridge Philosophical Society (Vol. 47, No. 2, pp. 396-400). Cambridge University Press.

Shin, D.H. and Sharma, M.M., 2014, February. Factors controlling the simultaneous propagation of multiple competing fractures in a horizontal well. In SPE Hydraulic Fracturing Technology Conference. Society of Petroleum Engineers.

Shou, K. J. 1993. A high order three-dimensional displacement discontinuity method with application to bonded half-space problems. Ph.D. thesis, University of Minnesota, Minnesota.

Simonson, E.R., Abou-Sayed, A.S. and Clifton, R.J., 1978. Containment of massive hydraulic fractures. Society of Petroleum Engineers Journal, 18(01), pp.27-32.

Sneddon, I., 1946, October. The distribution of stress in the neighbourhood of a crack in an elastic solid. In Proc. R. Soc. Lond. A (Vol. 187, No. 1009, pp. 229-260). The Royal Society.

Sneddon, I.N. and Elliot, H.A., 1946. The opening of a Griffith crack under internal pressure. Quarterly of Applied Mathematics, 4(3), pp.262-267.

Sophie, S.Y. and Sharma, M.M., 2018. A new method to calculate slurry distribution among multiple fractures during fracturing and refracturing. Journal of Petroleum Science and Engineering.

Teufel, L. W., and Warpinski, N. R. 1983. In-situ stress variations and hydraulic fracture propagation in layered rock-observations from a mineback experiment. In proceeding of the International Society for Rock Mechanics and Rock, Melbourne, Australia.

Thiercelin, M.J., Roegiers, J.C., Boone, T.J. and Ingraffea, A.R., 1987, January. An investigation of the material parameters that govern the behavior of fractures approaching rock interfaces. In 6th ISRM Congress. International Society for Rock Mechanics.

Ueda, K., Kuroda, S., Rodriguez-Herrera, A., Garcia-Teijeiro, X., Bearinger, D., Virues, C.J., Tokunaga, H., Makimura, D., Lehmann, J., Petr, C. and Tsusaka, K., 2018, January. Hydraulic Fracture Design in the Presence of Highly-Stressed Layers: A Case Study of Stress Interference in a Multi-Horizontal Well Pad. In SPE Hydraulic Fracturing Technology Conference and Exhibition. Society of Petroleum Engineers.

Valko, P. and Economides, M.J., 1995. Hydraulic fracture mechanics (Vol. 28). New York: Wiley.

Van Eekelen, H.A.M., 1982. Hydraulic fracture geometry: fracture containment in layered formations. Society of Petroleum Engineers Journal, 22(03), pp.341-349.

Warpinski, N.R., Schmidt, R.A. and Northrop, D.A., 1982. In-situ stresses: the predominant influence on hydraulic fracture containment. Journal of Petroleum Technology, 34(03), pp.653-664.

Warpinski, N.R., Moschovidis, Z.A., Parker, C.D. and Abou-Sayed, I.S., 1994. Comparison Study of Hydraulic Fracturing Models—Test Case: GRI Staged Field Experiment No. 3 (includes associated paper 28158). SPE Production & Facilities, 9(01), pp.7-16.

Weng, X., Kresse, O., Cohen, C.E., Wu, R. and Gu, H., 2011, January. Modeling of hydraulic fracture network propagation in a naturally fractured formation. In SPE Hydraulic Fracturing Technology Conference. Society of Petroleum Engineers.

Workman, A.D., Charvet, C.J., Clancy, B., Darlington, R.B. and Finlay, B.L., 2013. Modeling transformations of neurodevelopmental sequences across mammalian species. Journal of Neuroscience, 33(17), pp.7368-7383.

Wu, K., 2014. Numerical modeling of complex hydraulic fracture development in unconventional reservoirs. PhD Dissertation.

Wu, K. and Olson, J.E., 2015. Simultaneous multifracture treatments: fully coupled fluid flow and fracture mechanics for horizontal wells. SPE journal, 20(02), pp.337-346.

Wu, K. and Olson, J.E., 2015. A simplified three-dimensional displacement discontinuity method for multiple fracture simulations. International Journal of Fracture, 193(2), pp.191-204.

Xu, G. and Wong, S.W., 2013, March. Interaction of multiple non-planar hydraulic fractures in horizontal wells. In IPTC 2013: International Petroleum Technology Conference.

Yue, K., Olson, J.E. and Schultz, R.A., 2018, September. Layered Modulus Effect on Fracture Modeling and Height Containment. In Unconventional Resources Technology Conference, Houston, Texas, 23-25 July 2018 (pp. 3052-3071). Society of Exploration Geophysicists, American Association of Petroleum Geologists, Society of Petroleum Engineers.